CR-166280

CORRELATING MEASURED AND PREDICTED INPLANE STABILITY CHARACTERISTICS FOR AN ADVANCED BEARINGLESS ROTOR

By William H. Weller
January 1982

Prepared under Contract No. NAS2-10772 by

BELL HELICOPTER TEXTRON
Fort Worth, Texas

for

National Aeronautics and Space Administration

CORRELATING MEASURED AND PREDICTED INPLANE STABILITY CHARACTERISTICS FOR AN ADVANCED BEARINGLESS ROTOR

By William H. Weller
January 1982

CR-166280

Prepared under Contract No. NAS2-10772 by

BELL HELICOPTER TEXTRON
Fort Worth, Texas

for

AMES RESEARCH CENTER
NATIONAL AERONAUTICS AND SPACE ADMINISTRATION

TABLE OF CONTENTS

LIST OF TABLES

SUMMARY

A program of experimental and analytical research has been performed to demonstrate the degree of correlation achieved between measured and computed rotor inplane stability characteristics. The experimental data were obtained from hover tests for a scaled model of an advanced bearingless main rotor. Both isolated rotor and ground resonance conditions were tested. Test parameters included blade built-in cone and sweep angles, rotor inplane structural damping, pitch link location and fuselage structural damping. Analytical results for the conditions tested were obtained using current Bell Helicopter Textron analyses. In addition, variations in the analytical models were made to assess their impact on the correlation between computed and measured results. Results from this program are presented in tabular and graphical form in this report. The program documented herein was sponsored by contract (NAS2-10772) with the National Aeronautics and Space Administration, Ames Research Center.

INTRODUCTION

For more than two decades, both public and private sectors of the helicopter industry have tried to eliminate the requirement for main rotor bearings in an effort to reduce rotor weight, cost, and maintenance, while improving system reliability. Reference 1 presents an overview of the industry's efforts and the particular problems that had to be overcome. The approach has been to replace hub bearings with flexural elements, which deflect in accommodating blade motions. An evolution in multibladed rotor design has resulted: from articulated to hingeless, where lead-lag and flap bearings were replaced, to bearingless, where the pitch bearings were also eliminated. One distinguishing characteristic of hingeless and bearingless (non-articulated) rotors, when compared to articulated configurations, is their increased ability to transmit blade bending moments to the top of the mast and through it to the airframe. The rotor-fuselage coupling thus provided by the non-articulated hub significantly affects combined system dynamic stability. Ground resonance is one possible mode of instability as it involves inplane motions of the rotor blades and rigid body motions of the airframe. Even for an inflexible airframe (isolated rotor), kinematic coupling between the degrees of freedom of each blade can result in instabilities such as flap-lag and pitch-lag instability.

With regard to predicting non-articulated rotor characteristics, probably the greater effort has been directed toward development of analyses that could be used to determine isolated blade and coupled rotor-fuselage stability. References 2 through 5 illustrate some of the results achieved in this area for hingeless rotors, while reference 6 shows results for bearingless configurations. While predictions for articulated rotors have shown good agreement with measurements, correlation between measured and predicted characteristics of non-articulated rotors is worse as illustrated by reference 6. The fundamental problem lies in the fact that, unlike typical articulated rotors with a lag-flap-pitch hinge sequence, non-articulated rotors have virtual flap and lag hinges that rotate with blade feathering, thereby possibly creating large kinematic coupling effects. Other kinematic couplings may be intentionally induced through design. The structural design of a non-articulated rotor hub may even include redundant load paths. Finally, because of the higher effective hinge offsets typically associated with non-articulated rotors, blade elastic deflections are more pronounced. Analysis of non-articulated rotor stability, as well as many other characteristics, requires analytical tools reflecting a sensitivity to structural detail and aeroelastic effects that have been substantiated by comparison to experimental results.

Many companies within the helicopter industry have worked toward the development of viable non-articulated rotor systems. Bell Helicopter Textron (BHT) has developed numerous multibladed hingeless rotor systems to evaluate various design approaches. BHT's first flight test of a hingeless rotor occurred in 1957 (figure 1). In subsequent programs, other stiff-chordwise configurations were designed and tested, such as the one shown in figure 2. The development of viscoelastic materials, which could be efficiently used to provide high levels of inplane damping caused BHT to redirect their efforts toward soft-inplane configurations. This new emphasis on soft-inplane configurations with viscoelastic dampers contributed to the development of the Model 654 (reference 7 and figure 3) rotor. In 1977, BHT initiated a program to design and test a bearingless rotor. The bearingless hub would have a soft-flapwise and soft-chordwise flexure that, at its outboard end, provided little restraint to blade feathering motions imposed through flexure twisting. Damping was to be provided primarily through structural sources using elastomeric material.

Concurrent with these hingeless and bearingless rotor development programs, BHT has worked toward the establishment of inhouse analytical capabilities of sufficient accuracy to provide developmental support from preliminary design through flight test. The area of greatest difficulty has been predicting aeroelastic stability characteristics for hingeless and bearingless rotors. Past correlation attempts have, at times, yielded less than satisfactory results for both isolated rotor and ground resonance studies. As an example, figure 4 (which uses data appearing in reference 7) illustrates the correlation achieved in a study of the ground resonance characteristics of the M654 rotor using an earlier stability analysis. Although measured and predicted damping levels are comparable, some aspects of the measured trends are not matched by analysis, particularly because of the tendency of the analytical curve to depict a basic loss in damping as rotor speed is increased. It is thought that the failure to properly account for blade equilibrium position in determining elastic coupling effects could be a primary cause for the lack of correlation.

BHT has constructed a small-scale model of its current bearingless rotor design. For this model flap, lag, and torsional motions are accommodated in the hub flexure, which is bearingless, with the inplane motions also opposed by a damper-restrained, external cuff. Based on the use of this model, BHT has embarked on a program to conduct a new correlation attempt. In addition, both experimental and analytical results will be reviewed to obtain insight into the manner by which the particular physical characteristics of a bearingless rotor influence isolated rotor and ground resonance stability. The principal accomplishments of this program are discussed in this report. This program was performed in response to a contract (NAS2-10772) with the National Aeronautics and Space Administration, Ames Research Center. Dr. William Warmbrodt served as the Technical Monitor.

SYMBOLS

Units used for the physical quantities defined in this paper are given in the International System of Units (SI).

C_d	airfoil aerodynamic drag coefficient
C_ℓ	airfoil aerodynamic lift coefficient
C_m	airfoil aerodynamic pitching moment coefficient referenced to the quarter chord
f_b	blade inplane frequency, Hz
f_p	fuselage pitch frequency, Hz
f_r	fuselage roll frequency, Hz
K	inplane damper spring rate, N/m
I	natural mode generalized inertia, $N \cdot m \cdot s^2$
R	rotor radius
r_{PL}	radial station of pitch link to pitch horn attachment, cm
T	rotor thrust, g
β_b	built-in coning angle of blade (positive tip up), deg
γ_b	built-in sweep of blade (positive tip aft), deg
δ	natural mode damper shear deflection, m
δ_3	pitch-flap coupling angle (positive for pitch down with up flapping), deg
δ_4	pitch-lag coupling angle (positive for pitch up with lag), deg
ζ_b	blade inplane critical damping ratio (rotating system)
ζ_p	fuselage pitch critical damping ratio (fixed system)
ζ_r	fuselage roll critical damping ratio (fixed system)
ζ_s	blade inplane structural damping ratio (rotating system)

θ	blade collective pitch angle (positive nose up), deg
ϕ	blade damper material loss tangent angle, deg
Ω	rotor angular velocity, rad/s
ω	natural mode frequency, rad/s
Ω_{nom}	nominal rotor angular velocity, rad/s
$\bar{\Omega}$	rotor angular velocity normalized by the maximum value of 104.7 rad/s

EXPERIMENTAL APPARATUS AND PROCEDURES

The following paragraphs describe the bearingless rotor and fuselage models and the test procedures used during the experiments associated with this program. The rotor model is functionally the same as a full-scale rotor system under development at BHT. Major differences between the model and full-scale rotors include the inplane damper loss tangent (the ratio of material damping level to elastic spring rate) and blade design. The model hub, however, is an accurately scaled representation of the full-scale article. The model structural damping level, which is proportional to the damper loss tangent, is less than the full-scale value to yield more critical test conditions and, thus, data of greater interest in a study of this type. Model blade design variations from the full-scale design are believed to be of little consequence for this study.

Bearingless Rotor Model

The rotor model is a 2.42 m diameter, four-bladed, bearingless rotor with a maximum operating speed of 104.7 rad/s. Rotor flap, lag, and pitch motions are accommodated by flexural arms extending outward from the centerline to each blade. The blades are untwisted and untapered with center of gravities and shear centers located at the quarter chord. Other rotor geometric and structural properties are shown in tables I and II.

One unique feature of this rotor is the hub design, shown pictorially in figures 5a and 5b. The hub is formed by two flexural members, each continuing across the shaft attachment and connected to grips for opposite blade pairs. The two flexural members are stacked vertically and bolted to the mast at their centers. From the center of rotation, each flexural arm structurally

transitions into a flat flapping flexure and then into a torsionally soft feathering element with cruciform cross-section. The cruciform shape is carried to station 21.9 cm, at which point the arm was built-up to contain the bushings for attachment of the blade grips. A torsionally stiff cuff encompasses each flexure. The cuff, used to control blade feathering, is bolted to the blade grip at its outboard end. The cuff is shear restrained to the flexure at its inboard end (6.1 cm from the rotor center). The shear restraint mechanism is pinned in three directions, provides a beam shear load path to minimize beam-torsion coupling and flexure loads that would result from pitch link shears, and contains elastomeric shear pads for inplane damping augmentation (fig. 5b). The cuff has an integral pitch horn. Pitch link loads introduced to the horn will be reacted at the shear restraint in such a way as to generate a torsional couple, thereby rotating the cuff and twisting the attached flexure. The shear restraint rotates in pitch with the cuff and blade (fig. 5b). With the blade and flexure at flat pitch, the shear restraint mechanism is rotated -11° (nose-down).

Two sets of blade grips can be used, providing either 0 or 1.5° coning angles. Blade sweep of 0 or 2° aft can be achieved through the use of eccentric bushings pressed into the inboard blade attachment blocks. The pitch horn is oversized to accommodate pitch link radial station changes by the use of various spacer arrangements. Two sets of inplane dampers were tested. Both have spring rates of 595.4 N/cm, but with loss tangents of 0.246 and 0.33. The rotor structural damping level was proportional to the particular damper loss tangent value.

Two adjacent flexure arms are instrumented with four-arm strain gage bridges. Beamwise and chordwise bending moments are obtained at 3.1 and 5.9 percent radius and the flexure torsion is measured at 6.5 percent. The pitch link axial force and mast drive torque are also measured by strain gage bridges. Engineering load equivalents were recorded periodically with the data by using standard voltage level signals for each channel and noting the associated load level.

The model rotor is designed for Froude scale operation in air at atmospheric pressure based on a full-to-model scale factor of 5. Although compressibility and viscous effects on measured data are not representative, both static and dynamic deflections are properly simulated and the latter are more important for rotor stability testing. Scale factors relating the conceptual full-scale rotor to the model tested are listed in table III. Elastic simulation is based on matching the ratios of blade natural frequency to rotor speed. The calculated first inplane and out-of-plane frequency ratios for a nominal speed (81.7 rad/s) and moderate collective pitch (7°) are 0.74 and 1.04 per rev.

Fuselage Model

The fuselage model and drive system are shown in figures 6 and 7 which illustrate the more important features. The frame consists of an attachment shell, ballast support arms and rotor control system. The frame is mounted on a gimbal ring which, in turn, is connected to the drive stand. Connections between the frame shell, gimbal ring and stand are accomplished by soft flexures that have very low rotational stiffness and damping. The flexures provide fuselage freedom of motion in pitch and roll with respect to the drive stand. Linear springs and adjustable viscous dampers are attached between the stand and fuselage or gimbal ring to tailor fuselage frequencies (pitch and roll spring rates) and damping levels. Ballast weights are mounted on the support arms to appropriately model the fixed-system inertia.

The rotor shaft is direct driven by a variable-speed hydraulic motor. The motor is mounted within the lower portion of the drive stand, immediately above the thrust balance. A drive shaft is used to connect the motor with the rotor mast, extending through the fuselage shell with two universal joints to accommodate fuselage motion.

The model has a complete rotor control system driven by remotely controlled electric motors. Two actuators, arranged 90° apart, are used to control cyclic blade feathering, and a single actuator is used for collective pitch. Linear potentiometers sense swashplate position and, therefore, rotor trim state. For the isolated rotor testing, one cyclic actuator was replaced by a spring-loaded stop. The spring holds the swashplate against the stop to maintain zero cyclic pitch during normal operation. When rotor excitation was desired, the swashplate was pulled down against the spring and released. The resulting cyclic feathering input led to a transient lead-lag motion of the blade.

The fuselage and drive stand are instrumented to read fuselage motions, rotor trim state, speed, thrust and torque. The gimbal rotary flexures are strain-gaged to measure fuselage pitch and roll motions. The linear potentiometers, connected to the swashplate, provide rotor trim state data. Rotor thrust is measured by using a single component strain-gage balance mounted below the drive stand. Drive shaft torque is also sensed using a strain gage. Rotor shaft speed and azimuth position are determined using 1 and 60 per rev magnetic sensors. The rotating blade and shaft data are transferred to the fixed system through a 24-ring, slip-ring assembly using two brushes per ring. Rotor thrust, torque and trim positions are continuously displayed on analog meters mounted in a model operator's console. Rotor speed is read by using a frequency counter sensing the 60 per rev magnetic sensor signal.

The same fuselage and stand combination was used for both isolated rotor and ground resonance tests. In the case of the isolated rotor testing, additions to the model were made, as shown in figure 7, to provide a large hub impedance and eliminate the free-hub effect. The model snubber was raised and locked to secure the fuselage and a steel stabilizer frame was attached between the extremes of the ballast support arms and the drive stand base below the balance. These frames were also cross-braced. Above the rotor hub, a bearing-supported fixture was attached to the shaft and steel cables connected between the fixture and tie-down points in the test cell. The cables were tensioned with turnbuckles. The fixture allowed the shaft to turn, while restricting hub motion.

Test Procedures and Data Reduction

Rotor inplane stability characteristics were measured in a hovering condition for numerous rotor and fuselage configurations. Operating conditions were varied over wide ranges of rotor thrust (0-330N) and rotational speed (57-100 rad/s). The nominal values of 1g rotor thrust and rotational speed were 222.4 N and 81.7 rad/s, respectively. Each run was initiated by bringing the rotor speed up to the desired value and setting collective pitch to yield the specified thrust. Sustained first harmonic rotor flapping was eliminated during the test. Once the test conditions were established, the model was "plucked" and the transient response recorded on both oscillograph and magnetic tape recorders. For isolated rotor tests, the swashplate position was stepped using a spring-loaded stop mechanism which replaced one of the cyclic actuators. For ground resonance tests, the fuselage was excited by pulling on one of the ballast support arms at a point removed from both pitch and roll axes.

After transient data were recorded for a test point, the thrust and/or rotor speed was changed to the next value and the process repeated. The program consisted of data sets with varying thrusts at a constant rotor speed or varying speed at constant thrust. A few data sets were obtained showing a variation with rotor speed for a constant collective pitch. Five rotor configurations were tested and their parametric values are identified in table IV. In addition to the isolated rotor tests (designated as fuselage configuration F-1), two free-hub configurations were examined. Characteristics of the nominal fuselage case (F-2) are listed in table V. The second free-hub case (F-3) had both pitch and roll damping ratios equal to one-half those of case F-2, while all other parametric values were the same.

Appendix A lists the various combinations of rotor, fuselage and operating conditions that were examined. Note that the rotor speed, $\bar{\Omega}$, is normalized by the maximum allowed value of 104.7 rad/s. Rotor stability characteristics were recorded for each test point. Hub beam and chord bending moments at 0.031R, hub torsion at 0.065R and the pitch link axial force for adjacent blades and the hub chord moment at 0.059R for one blade were all recorded on magnetic tape. The fuselage pitch and roll motions and the 1 per rev rotor pulse signal were also recorded on magnetic tape. These same data channels were recorded by an oscillograph as well.

The oscillograph traces were analyzed to produce the stability data listed in Appendix A. Frequency was determined by peak counting the hub chord bending moment, fuselage pitch or roll motion traces. Damping ratio was calculated by applying the logarithmic decrement technique to the appropriate trace.

ANALYSIS AND MODIFICATIONS

The analytical research was performed using BHT computer programs DNAM06, DRAV21TF, and ARAM06. Program DNAM06 is the current production version of the BHT series of programs used to calculate blade modal characteristics. DRAV21TF is the production rotor stability analysis capable of determining both isolated rotor and ground resonance characteristics for hover. Program ARAM06 is a modified version of DNAM06, having in addition the determination of blade equilibrium position and its effects on the modal characteristics. A second option in program ARAM06 uses a transformation of bending and torsion moments, as well as slopes, to determine the elastic coupling effects that arise with blade coning and sweep. Descriptions of these programs and the modifications in developing and using program ARAM06 are presented in the following paragraphs.

Modal Analysis

The blade modal analysis is performed using the production version of BHT computer program DNAM06, which is documented in reference 8. Program DNAM06 is used to compute the fully coupled rotating natural frequencies and mode shapes of the rotor blade in vacuo. Blade flexibility is modeled by piecewise uniform, untwisted, massless elastic elements with principal axis misalignment and shear center and elastic axis offsets from the reference axis. The inertial properties are represented by lumped elements that have principal axes misaligned with the basic hub reference coordinate system; center of mass offsets

from the reference axis; and which undergo vibratory and centrifugal accelerations. Various combinations of blade pitch control system, pylon impedance, and hub structural detail can be modeled to represent the effects of most realistic hub configurations. The program calculates modal qualities assuming five degrees-of-freedom (radial vibrations are ignored). Program inputs include rotor geometry (radius, chord, twist, pitch link location, etc.), hub and blade structural parameters (mass, mass moment, and bending and torsional stiffness distributions), hub impedance parameters, and rotor operating conditions (rotor speed and blade pitch). The DNAM06 program is capable of modeling the redundant structural details of a bearingless rotor with shear restrained cuff, such as that used in this program.

Program DNAM06 does not account for the effects of preconed or prelagged hub flexures or coned and swept blades on the blade modal characteristics. It also does not analyze the blade in its operating position deformed by the action of its load environment. It is left for subsequent analyses to account for these effects. As discussed in reference 4, these geometric qualities, as well as the blade's position, do affect inplane stability characteristics by virtue of an induced elastic flap-lag-torsion coupling.

The structural damping that arises from the cuff inplane restraint is computed based on results from program DNAM06. In that analysis the inplane structural damping ratio, normalized by damper material loss tangent, is computed for each mode based on the following relationship.

$$\frac{\zeta_s}{\tan \phi} = \frac{K\delta^2}{2I\omega^2}$$

Only the normalized damping ratio computed for the first inplane mode is used for subsequent stability analysis.

Stability Analysis

Isolated rotor and ground resonance stability characteristics are predicted by the production version of BHT computer program DRAV2 TF which is an eigenvector analysis similar to the DRAV02 program documented in reference 9. DRAV21TF interfaces with program DNAM06 to model the elastic rotor by using up to ten fully coupled modes calculated by the latter program. In contrast, program DRAV02 uses a lumped mass and spring-restrained hinge representation for the blade. The fixed-system representation in DRAV21TF models both the pylon and fuselage as lumped masses,

moments of inertia, and hinges having spring and damper restraint. The various elements are connected by massless, rigid rods. Pitch and roll of both the pylon and fuselage and combined system lateral and longitudinal translation are allowed. For this program, the analytical model considered only fuselage pitch and roll motion as illustrated in figure 8. The rotor and fixed system are coupled by virtue of the hub shears and moments. The analysis treats various articulated, hingeless and bearingless rotor configurations and includes such parameters as hub precone and prelag; blade droop and sweep; and spanwise variations of center of gravity and aerodynamic center offsets, blade twist and chord.

Quasi-steady aerodynamic loads are derived from tabulations of C_ℓ, C_d, and C_m using a table look-up process dependent on local Mach number and aerodynamic angle of attack. A program option allows the use of nonlinear equations to formulate the aerodynamic coefficients. For this study, the optional equations were used to define the aerodynamic coefficients by

$$C_\ell = 5.73\alpha$$

$$C_d = 0.008 + 0.179\alpha^2$$

$$C_m = 0$$

where α is the aerodynamic angle of attack in units of radians. The aerodynamic loads are calculated using strip theory and neglecting radial flow effects. A dynamic inflow model is provided for optional use. Fuselage aerodynamic loads are neglected.

For this program the stability analysis made use of the rotating first and second inplane mode, the first three flap modes and the first torsion mode. The structural damping for the first inplane mode was based on the normalized damping ratio from program DNAM06 and the loss tangent of the inplane damper material for the particular rotor configuration in question. For the other five modes the structural damping ratio was assumed to be 0.02.

A numerical iteration procedure is used to calculate the blade equilibrium position based on a linearized set of equations. These same equations, but with time dependent terms retained, are used in the perturbation analysis. Terms, such as those which are nonlinear in nature and not included in the modal analysis, are treated as forcing functions in the stability equations. The blade perturbation equations are transformed from the rotating coordinate system to the fixed system, using a multiblade coordinate transformation to eliminate the periodic coefficients

from the equations of motion. The solution is based on the normal mode approach using generalized coordinates associated with each rotor mode and the selected fixed-system motions.

The modal analysis, program DNAM06, includes only linear terms that arise from the structural character of a rotor blade. In the stability analysis, the resulting modes are first used in conjunction with static aerodynamic forcing functions to calculate the blade's equilibrium position for a hovering condition. For the subsequent stability analysis, certain nonlinear effects have been modeled to more completely describe the elastic bending and torsion motions of the blade. Differential equations 61(b), (c), and (d) of reference 10 contain higher order terms involving spatially differentiated elastic displacement variables. Because these terms were not included in the modal analysis, the stability equations have been formulated to reflect these nonlinear effects. These particular terms of reference 10 have been linearized about the blade equilibrium position to produce products of static and oscillatory bending curvatures. The static curvatures are defined from the calculated blade equilibrium position. The oscillatory curvatures are expressed in terms of the input mode shapes by differentiating the slopes computed in program DNAM06. These nonlinear terms introduce elastic torsional moments in the equations of motion that arise from moderate bending deflections and are combined with the aerodynamic loads as generalized forcing functions of the normal modes calculated by DNAM06. These bending curvature terms are included in the basic stability analysis except for specific cases where their omission is pointed out. Built-in blade coning effects are included in the calculated equilibrium position. Other than that and the above described curvature terms, blade coning is not explicitly included in the stability calculations.

Analytical Modifications

Program DNAM06 calculates modal characteristics based on a straight line hub and blade axis aligned perpendicular to the shaft axis about which elastic twisting is assumed. This does not allow such design parameters as hub precone and prelag, as well as blade built-in coning and sweep, to be modeled. Further, the influence of blade equilibrium position is not accounted for at this stage of the analysis. Thus, the modal characteristics predicted by DNAM06 do not fully reflect the elastic flap-lag-torsion coupling effects described in reference 4 and which are dependent on hub design and rotor operating condition. As shown by reference 4, analysis of complex rotor systems which are aeroelastically sensitive to elastic and kinematic couplings, such as the bearingless rotor, should correctly model the position of the blades relative to the axis of rotation and to the

feathering element of the hub. This may be more readily accomplished during modal analysis of the rotor rather than during subsequent stability or response analysis.

Consequently, program DNAM06 was modified to allow these elastic coupling effects to be more fully represented. An existing static equilibrium analysis, reference 11, was incorporated into the program code. The resulting program, ARAM06, is used in lieu of DNAM06 and in conjunction with DRAV21TF for the modified analysis. ARAM06 uses both operating and design parameters to compute the blade equilibrium position. Hub precone and prelag and blade droop and sweep effects on the equilibrium conditions are included in the analysis as indicated by the schematic in figure 8. The determination of equilibrium position reflects the spanwise variations in blade twist, structural stiffness, weight, center-of-gravity and neutral axis offsets from the reference axis, and section radius of gyration. Rotor speed and collective pitch describe the operating conditions. The pitch-horn and cuff geometries are also specified. All geometric and load discontinuities occur at segment junctions or nodes. Airloads are calculated by assuming a triangular lift distribution with the magnitude calculated by strip theory.

To determine the static equilibrium position about which the modes are superimposed, a tension-beam analysis is performed to calculate blade shears and moments about the principal axes at the spanwise center of each segment. The resulting deflections of the blade from its initial position are calculated. By iteration, the final static equilibrium position of the blade relative to the mast coordinate system and corresponding shears and moments are computed. These data form a consistent set of shears, moments, displacements and slopes to be used in the DNAM06 analysis. Analytical representations also include a cantilevered hub, lumped-mass representation of each segment, and symmetrical airfoil. Blade torsion is uncoupled from the beam and chord degrees of freedom except for the control system effects.

The resulting elastically deformed equilibrium position of the blade is used to define incremental center of gravity, shear center, and neutral axis offsets from the designated elastic feathering or pitch change axis. For this study, the pitch change axis is defined as being tangent to the blade equilibrium position at a radial station of 14 cm from the centerline. These offsets, added to the input cross-section values, are used in conjunction with the basic equations of motion of program DNAM06 to reflect elastic couplings between the flap, lag, and torsional degrees of freedom in program ARAM06.

As will be shown in a subsequent section, one basic shortcoming of the previously described approach is that a single pitch change axis is used from which the equilibrium position of the complete blade is referenced. This single coordinate system representation leads to large offsets for the outboard blade segments and the resulting dynamic torsional moments become excessive at higher thrust conditions. These offsets are made even larger due to the introduction of blade sweep or coning. The end result is that the elastic twist, reflected in the first flap and lag modes, due to blade coning and sweep effects is overpredicted. A second modified modal analysis approach was, therefore, formulated.

In this alternative modified modal analysis, the equilibrium position of the blade, including the built-in blade sweep and coning angles, is used to perform a transformation on the dynamic bending and torsion moments and slopes calculated by the equations of motion from DNAM06. The transformation is performed as the analysis is stepped over the region between the radius where precone is applied to the radius where coning and sweep are applied. Analogous transformations for shears and deflections are neglected because their effect is expected to be significantly smaller. When the transformation approach is used, the offsets related to the equilibrium position, used in the original modified analysis, are neglected. The modal data from both modified approaches were used in the production stability analysis with the bending curvature terms deleted. The inplane structural damping ratio, used in the stability calculations, is approximately the same for both basic and modified analytical approaches as shown in table VI.

PRESENTATION OF RESULTS

The results of the experimental and analytical research using the basic analysis, are presented in Appendices A and B, respectively. Representative measured and calculated results are presented graphically in figures 9 to 29 and discussed in subsequent paragraphs. In the appendices the inplane damping and frequency are expressed as rotating coordinate system values. In the figures, the inplane frequency is shown in the rotating system for isolated rotor conditions and fixed system for ground resonance cases, while the damping is presented exclusively in the rotating system. All other damping and frequency values in the appendices and figures are expressed in the fixed system. With the exception of figures 21 to 27, the calculated results are from the basic production analyses, using DNAM06. The organization of the figures is as follows:

DISCUSSION OF RESULTS

Isolated Rotor Analytical Correlation

Comparisons of measured and calculated isolated rotor inplane characteristics are illustrated for rotor configuration R-1 in figures 9, 10, and 11. In the figures, 1g thrust refers to a value of 222.4 N. The calculated results are obtained from the production analyses, DNAM06 and DRAV21TF. In figures 9 and 10 the dashed curves represent the inplane mode calculated structural damping ratio which is the same for rotor configurations R-1, R-2, and R-4 and is tabulated in table VI. The damping ratio for R-6 and R-7 is approximately three-fourths of the values in these figures and table. This structural damping is derived from the modal analysis (DNAM06) and based on the loss tangent of the shear restraint damper material. The structural damping is nearly invariant with thrust (collective pitch) and decreases slightly with increasing rotor speed. The latter trend is due mostly to the centrifugal stiffening of the flexure causing it to carry a greater portion of the inplane bending moments. The difference between the solid and dashed curves of figures 9 and 10 represent the contributions that arise from aeroelastic sources and from coupling with other modes.

As shown in figure 9, the agreement between measured and calculated inplane frequency is good both in regard to value and trend. The calculated damping is unconservative and shows a larger discrepancy at the lower rotor speeds. This trend is further illustrated by the data of figure 10. As rotor speed is decreased, the predicted damping curves show a significant increase in aeroelastic sensitivity to thrust level, the degree of which is not reflected by the test data. One source of this stabilizing aeroelastic contribution in the analysis is illustrated by figure 11 which reflects the contribution of the static bending curvature terms of program DRAV21TF. While their effect on inplane frequency (not shown) is insignificant, the greater impact is on the damping trends. The contribution of these terms increases with thrust and decreasing rotor speed, as the bending curvature of the blade axis is increased. Exclusion of these terms greatly improves the agreement between measured and calculated results.

Even with the exclusion of the bending curvature terms, the correlation is not good at the lowest rotor speed condition as shown in figure 11. With the exception of the first coupled inplane mode, the only mode with significant participation in the inplane response is the highly damped first coupled flap mode. The contribution from this mode increases at the lower speeds where the first flap and lag modes are nearly resonant. Calculated inplane damping in this operating speed range is sensitive to the relative magnitude and phasing of the first inplane and flap mode contributions. At the highest rotor speed, where the effect of the first flap mode is minimal, the damping correlation is best. Even at the lowest speed, the difference between measured and calculated damping is not large allowing for scatter in the test data.

Variations in analytical correlation between the different rotor configurations are shown in figures 12 to 15. The production analyses incorrectly reflect the effects of blade coning as suggested by the data of figure 12. As shown in references 1 and 6, blade coning is stabilizing For the test model with its small flap virtual hinge offset, the effect of coning is less than that for rotors with larger offsets. The effect, however, is discernible, adding a damping increment of approximately 0.005 as shown in figure 12. As shown in figures 13 to 15, the damping trends with blade sweep, structural damping and pitch link location are generally well-predicted by the analysis, although the stability increments differ between the measured and predicted data. The one exception is the effect of pitch-link location (δ_3) for moderate thrust levels.

From figures 12 to 15, the previously observed trend of unconservative damping predictions at the lower rotor speed condition occurs consistently with all rotor configurations. In the analysis the bending curvature contributions are not greatly sensitive to these rotor design parameters. Similarly, the first flap mode contribution will generally be affected only in a secondary manner. For all isolated rotor damping predictions at constant rotation speed, decreasing rotor thrust yields an increase in damping at the low thrust levels. This is not seen in the measured data, although the accuracy of the measured data is more subject to question at the low thrust condition. These discrepancies between measured and predicted trends should be further investigated.

Ground Resonance Analytical Correlation

The correlation between measured and calculated ground resonance characteristics for rotor configuration R-1 and fuselage configuration F-2 is depicted in figures 16 and 17. The frequency correlation shown in figure 16 for the blade is excellent, although the fixed-system frequencies are slightly underpredicted. This yields an underprediction of the resonance condition by approximately $0.03\bar{\Omega}$. Based on this latter observation, a limited study was performed to examine in greater detail the fixed-system frequency trends. It was found that the analysis correctly predicts the nonrotating (uncoupled) body frequencies both with and without the rotor inertia effects. The increased rotor hub restraint of the body motions that arises as rotor speed is increased was also verified in the analysis. One area that was not studied is the action of rotor thrust on body motions. Even so, it is felt that the frequency correlation is adequate.

The damping comparison of figure 16 repeats the trend observed in the isolated rotor data. The predicted damping is unconservative at the lower rotor speed conditions. The damping "buckets" occur at the same rotor speed values. At the higher speed range, where the effects of the first flap mode are minimal, the damping correlation is good. However, the predicted relative minimum damping points do not occur at predicted frequency resonances between the inplane and fuselage modes. This discrepancy is, as yet, unexplained.

Aeroelastic sensitivity with thrust and rotation speed of the rotor damping characteristics for the free-hub condition is illustrated by figure 17. For the lowest rotor speed condition, the predicted damping is higher than the measured values with the amount being slightly influenced by the thrust level. The contribution from the static bending curvature terms included in the stability analysis is not as significant for the free-hub case in comparison to their effects for the isolated rotor condition as shown in figure 11. In fact, the bending curvature contribution for a free-hub and at the lowest rotor speed is negligible. The discrepancy between measured and predicted damping for this case is possibly due to the relative first flap mode influence on the inplane response which is significantly greater for a free-hub condition, as reflected by the calculated eigenvectors. For the two higher rotor speed conditions, the effect of the bending curvature terms, as shown in figure 17, is inconclusive as to whether their inclusion in the analysis improves correlation. In either case, the damping correlation at these rotor speed conditions is adequate.

Comparisons of measured and predicted damping trends for the various rotor configurations and a free-hub condition (F-2) are presented in figure 18. Although test data scatter prohibits a clear interpretation of the effect of blade coning, it is felt that its influence is stabilizing, if effective at all, for a free-hub condition in contrast to the destabilizing analytical projection. This analytical trend is relatable to the similar isolated rotor trend where the analytical and experimental trends with blade coning were opposite, although the analytical trend was very slight. The analytical trends with blade sweep and pitch-link location (δ_3) more closely match experimental results. The sensitivity of the effects of these two parameters with thrust differs, however, between analytical and experimental curves.

The correlation for points of neutral or negative stability is demonstrated in figures 19 and 20. The minimum damping values associated with the rotor inplane and body roll resonance ($\bar{\Omega}$ = 0.7) are not suitably predicted by the analysis. The primary reason may be the damping contribution from the first flap mode which prevails over the lower rotor speed range. The negative and neutral stability conditions projected by the test data at $\bar{\Omega}$ = 0.7 and shown in figures 19 and 20 are not predicted by the analysis. The inplane and body pitch resonance damping levels are reasonably predicted over the range of 0.9 to 0.95 for $\bar{\Omega}$. Again, at these speeds, the influence of the first flap mode on the inplane response is minimal.

Modified Analysis Correlation

The correlation, based on the modified modal analysis (using the blade equilibrium position as discussed under Analytical Modifications), is shown in figures 21 and 22 at nominal rotor speed for isolated rotor and ground resonance conditions respectively. From figure 21, the inclusion of the equilibrium position model in the modal analysis causes the resulting predicted damping ratio values to correctly reflect a stabilizing trend with blade coning in contrast to the results from the basic analysis (figure 12). At 1.4g thrust, however, the measured and modified analysis damping ratio increments that arise from blade coning are approximately 0.005 and 0.013, respectively. Further, the measurements suggest that at moderate thrusts the influence of blade coning is significantly diminished, if not eliminated, for a free-hub condition as shown in figure 22. The modified analysis predicts a free-hub damping increment of 0.009 at a 1.4g thrust. The addition of the equilibrium position model in the modal analysis has, therefore, overcorrected for the blade coning effect.

Examination of the mode shapes calculated by the modified analysis suggests that the most significant influence of blade coning is the induced elastic twist in the first inplane mode. This elastic δ_4, nose-up with lag sense, when applied to a thrusting rotor, leads directly to an increase in computed damping level. Even for the configuration without built-in blade coning, R-1, the elastic blade coning at the higher thrusts causes a similar effect of increasing elastic twist which degrades the correlation. The deformed equilibrium positions of the blade flap deflections for configurations R-1 and R-2, calculated by the modified analysis, are presented in figure 23. The positions are very similar, except for the coned blade having a slightly higher elevation and the bending curvatures in the area of the built-in cone angle (22 percent radius). These subtle differences in position lead to the different elastic twist characteristics to which the predicted damping is sensitive. The tendency of the modified analysis to overpredict the effect of blade elastic coning on the damping for configuration R-1 perhaps results from the fact that a single pitch change axis system (tangent to the blade at 11.5 percent radius) is used to compute center of gravity and shear center offsets for all stations. While this representation might adequately represent hub flexure twisting, it leads to overpredictions for the elastic twists of the blade segments because of their large offsets. Thus, while the methodology of using an equilibrium position to reference mode shapes may be correct, this specific illustration has failed to substantiate that fact.

The difference in the computed equilibrium positions of the blades for R-1 and R-2 suggests that a more subtle effect is required. Based on the calculated equilibrium positions for configurations having built-in blade coning and sweep, an alternate approach was formulated. It is likely that the most significant difference in the positions for R-1 and R-2 is in the different curvatures and slope discontinuity that occur in the region around 22 percent radius where the blade coning is applied. A similar observation can be made for the inplane position of the blade with respect to the application of blade sweep. It was therefore proposed that a transformation of the dynamic bending and torsion moments be made as the modal analysis is stepped over the region of the blade where coning and sweep are applied. The transformation would be used to account for elastic coupling between the bending and torsion degrees of freedom that arise as a result of applying blade sweep and coning.

The results from using the modified modal analysis based on the transformation approach are reflected in figures 24 to 27. In figure 24 the correlation of blade coning effects is shown. The agreement between measured and predicted values as to the increment in damping that results is excellent for thrust levels

greater than 0.2g and the projected damping levels are in close agreement at the higher thrusts. The correlation is certainly improved over that using the basic analysis. As shown in figure 25, the destabilizing damping increment that results from blade sweep is similar for both basic and modified analyses with the basic analysis yielding slightly better absolute damping estimates. Again, the correlation for both analyses is better at the higher thrusts. For the free-hub condition of figure 26, the damping increment due to blade coning as calculated by the modified analysis is still excessive and reflects a trend opposed to the basic analysis results. For both configurations R-1 and R-2 under a free-hub condition, the modified analysis predicts a destabilizing trend with thrust in agreement with the test data. However, the basic analysis shows no significant change in damping for thrust levels higher than 0.8g.

The correlation that results from use of the modified analysis based on the moment transformation is shown in figure 27 over the range of rotor speeds examined in this study. It can be observed in this figure that the correlation for both rotor configurations R-1 and R-2 has been generally improved. The discrepancy between measured and calculated results for configuration R-1 and at the lower rotor speeds has been diminished by use of the transformation analysis. Some difference remains, however, possibly arising from the influence of the first flap mode. The measured increment in damping ratio due to blade coning is also reasonably reproduced by the modified analysis in contrast to the predictions associated with the basic analysis.

Additional Rotor Stability Trends

One characteristic of this rotor model which significantly influences the stability trends is the pitch inclination angle of the shear restraint relative to the flexure axes, illustrated by schematic in figure 5b. As previously described, the cuff is fixed at its outboard end to the blade and hub flexure interface hardware. At its inboard end it is connected to the flexure through a shear restraint and inplane damper mechanism. The mechanism is pinned to the flexure to allow free feathering with cuff pitching motions. When the flexure and blade are at flat pitch, the damper is inclined, or indexed, 11° nose-down from a vertical axis. At this point, aft bending of the blade causes a forward shearing of the damper and the inboard end of the cuff is lowered by virtue of the damper axis inclination. Because the pitch horn is mounted to the trailing side of the cuff at its inboard end, the lowering of the cuff will lead to an induced negative pitch angle creating a kinematic δ_4 effect. As collective pitch is increased, the angle between the shear restraint

axis and the vertical is decreased until pitch angles in excess of 11° are reached, as illustrated in table VI. For collective pitch angles below 11° the nose-down with lag induced pitch will destabilize the rotor, as shown in figure 28, over a large portion of the operating thrust range. With the exception of the data of figure 28, the effects of blade index angle were always included in the analysis.

The computed effect of softening the control system is illustrated by figure 29. The reduced control system springrate was one-half the nominal value and created a stabilizing influence that increased with thrust beyond the point of minimum damping. This trend is supported by reference 4, where the discussion points out that in the presence of favorable aeroelastic coupling a reduced control system springrate will enhance stability. The magnitude of the increase in damping will depend on the degree of favorable aeroelastic coupling that is present.

CONCLUDING REMARKS

A program of experimental and analytical research has been performed to demonstrate the degree of correlation achieved between measured and computed rotor inplane stability characteristics. The experimental data resulted from hover tests for a 1/5-scale model of an advanced bearingless main rotor. Both isolated rotor and ground resonance conditions were tested over the model operational rotor speed and thrust ranges. Rotor inplane frequencies and damping were obtained, as well as similar characteristics for the fuselage pitch and roll degrees of freedom when applicable. A number of rotating and fixed-system parameters were varied during the tests. These included blade built-in coning and sweep angles, rotor inplane structural damping, pitch link location and fuselage structural damping. Analytically derived results for the same test conditions were obtained using current BHT in-house analyses.

The analyses used in this program included a rotor modal analysis, program DNAM06, and an inplane stability analysis, DRAV21TF. Variations in the analytical models were made to assess their impact on the correlation between computed and measured results. One of the variations was the modification of the modal analysis to include the effects of the blade operational equilibrium position on the subsequently calculated mode shape and stability characteristics.

Assessment of the computed and measured results showed general agreement between them, particularly with regard to frequency trends. The computed effects of blade coning did not agree with measured characteristics. Also, the inplane damping predictions were unconservative over the lower range of rotor speeds tested. The inclusion of the equilibrium position in the modal analysis improved the trend with blade coning, although better results were achieved with other program modifications. The unconservative damping predictions are thought to arise from the coupling between the first inplane mode and the highly damped first flap mode.

APPENDIX A

EXPERIMENTAL OPERATING CONDITIONS AND ASSOCIATED STABILITY CHARACTERISTICS

Rotor Conf.	Fuse. Conf.	$\bar{\Omega}$	T g	θ deg	f_b Hz	ζ_b	f_r Hz	ζ_r	f_p Hz	ζ_p
R-1	F-1	.65	0.16	3.5	9.3	.0220	(Isolated Rotor Test)			
		.65	0.30	5.0	9.2	.0223				
		.65	0.60	7.7	9.0	.0248				
		.65	0.92	10.0	8.9	.0278				
		.65	1.28	13.0	8.9	.0316				
		.78	0.14	3.2	9.7	.0172				
		.78	0.28	4.2	9.7	.0191				
		.78	0.34	4.9	9.7	.0194				
		.78	0.62	6.4	9.7	.0205				
		.78	0.64	6.8	9.6	.0211				
		.78	0.92	7.8	9.6	.0233				
		.78	1.02	8.8	9.6	.0235				
		.78	1.24	9.9	9.6	.0260				
		.78	1.28	10.2	9.4	.0274				
		.78	1.42	11.0	9.2	.0293				
		.78	1.46	11.2	9.4	.0302				
		.90	0.16	3.3	10.0	.0180				
		.90	0.24	3.8	10.1	.0191				
		.90	0.60	5.7	10.0	.0200				
		.90	0.92	7.0	9.7	.0208				
		.90	1.24	8.1	9.7	.0221				
		.90	1.42	9.0	9.8	.0230				
		.65	1.00	10.0	9.2	.0260				
		.78	1.04	7.8	9.6	.0229				
		.85	1.04	7.0	9.8	.0211				
		.90	1.00	6.4	9.9	.0203				
		.95	0.98	6.0	10.1	.0198				
		.60	0.52	7.8	9.0	.0300				
		.65	0.60	7.8	9.1	.0270				
		.70	0.68	7.8	9.2	.0263				
		.75	0.78	7.8	9.3	.0260				
		.78	0.86	7.8	9.4	.0253				
		.80	0.90	7.8	9.4	.0253				
		.85	0.98	7.8	9.7	.0235				
		.90	1.10	7.8	9.8	.0230				
		.95	1.18	7.8	9.9	.0216				

APPENDIX A (Continued)

Rotor Conf.	Fuse. Conf.	$\tilde{\Omega}$	T g	θ deg	f_b Hz	ζ_b	f_r Hz	ζ_r	f_p Hz	ζ_p
R-2	F-1	.65	0		9.1	.0244	(Isolated Rotor Test)			
		.65	0.32		9.2	.0262				
		.65	0.68		9.3	.0282				
		.65	1.00		9.2	.0310				
		.65	1.24		8.9	.0368				
		.78	0.38		9.7	.0217				
		.78	0.72		9.8	.0233				
		.78	1.04		9.5	.0279				
		.78	1.36		9.3	.0333				
		.78	1.48		9.3	.0362				
		.65	0.98		9.1	.0317				
		.78	1.00		9.4	.0274				
		.85	1.00		9.6	.0250				
		.90	0.98		9.9	.0232				
		.95	0.94		10.1	.0224				
		.65		7.7	9.1	.0312				
		.78		7.7	9.4	.0270				
		.85		7.7	9.7	.0251				
		.90		7.7	9.8	.0238				
		.95		7.7	10.0	.0230				
R-4	F-1	.78	0.30		9.8	.0152				
		.78	0.58		9.8	.0168				
		.78	0.92		9.5	.0197				
		.78	1.12		9.7	.0227				
		.78	1.30		9.3	.0269				
		.60	0.96		8.9	.0263				
		.65	0.92		9.1	.0221				
		.78	0.94		9.7	.0194				
		.85	0.86		9.9	.0183				
		.90	0.88		10.1	.0175				
		.95	0.82		10.3	.0166				
R-6	F-1	.78	0.16		9.4	.0171				
		.78	0.32		9.3	.0177				
		.78	0.64		9.3	.0187				
		.78	0.96		9.2	.0207				
		.78	1.28		9.2	.0228				
		.78	1.44		9.2	.0245				
		.65	0.96		8.8	.0255				
		.70	0.96		9.0	.0226				
		.75	0.96		9.1	.0213				
		.78	0.96		9.3	.0204				
		.80	0.96		9.4	.0195				
		.85	0.96		9.5	.0178				
		.90	0.96		9.7	.0152				
		.95	0.96		10.0	.0125				

APPENDIX A (Continued)

Rotor Conf.	Fuse. Conf.	$\bar{\Omega}$	T g	θ deg	f_b Hz	ζ_b	f_r Hz	ζ_r	f_p Hz	ζ_p
R-7	F-1	.78	0.16		9.4	.0187	(Isolated Rotor Test)			
		.78	0.32		9.4	.0200				
		.78	0.64		9.3	.0215				
		.78	1.28		9.2	.0300				
		.78	1.44		9.2	.0330				
		.60	0.96		8.9	.0289				
		.65	0.96		9.0	.0286				
		.70	0.96		9.1	.0260				
		.75	0.96		9.2	.0242				
		.78	0.96		9.3	.0237				
		.80	0.96		9.4	.0228				
		.85	0.96		9.6	.0218				
		.90	0.96		9.7	.0203				
		.95	0.96		9.9	.0196				
R-1	F-2	.65	0.16		8.9	.0194	2.3	.119	5.2	.100
		.65	0.32		8.8	.0191				
		.65	0.64		8.7	.0171				
		.65	0.96		8.7	.0137				
		.65	1.28		8.5	.0098				
		.78	0.16		9.8	.0153	2.5	.152	4.8	.100
		.78	0.32		9.8	.0149				
		.78	0.64		9.8	.0115				
		.78	0.96		9.6	.0107				
		.78	1.28		9.7	.0095				
		.78	1.44		9.7	.0081				
		.90	0.16		10.0	.0070	2.4	.126	5.3	.091
		.90	0.32		9.9	.0058				
		.90	0.64		9.9	.0047				
		.90	0.96		9.8	.0051				
		.90	1.28		9.8	.0049				
		.90	1.44		9.8	.0047				
		.55	0.96		9.1	.0231	2.5	.134	5.0	.090
		.60	0.96		8.7	.0253	2.4	.145	4.9	.095
		.65	0.96		8.7	.0140	2.3	.109	4.9	.137
		.70	0.96		9.1	.0031	2.5	.023	4.9	.103
		.75	0.96		9.5	.0062	2.7	.052	4.8	.110
		.78	0.96		9.7	.0099	2.8	.069	5.0	.091
		.80	0.96		9.7	.0102	2.5	.148	5.0	.090
		.85	0.96		9.9	.0106	2.3	.149	5.0	.094
		.90	0.96		9.8	.0051	2.4	.149	5.1	.048
		.95	0.96		10.2	.0059	2.4	.115	5.1	.052
		.60		7.8	8.8	.0230	2.3	.165	4.9	.119
		.65		7.8	9.0	.0140	2.2	.133		

APPENDIX A (Continued)

Rotor Conf.	Fuse. Conf.	$\tilde{\Omega}$	T g	θ deg	f_b Hz	ζ_b	f_r Hz	ζ_r	f_p Hz	ζ_p
R-1	F-2	.70		7.8	9.2	.0044	2.5	.024		
		.75		7.8	9.4	.0061	2.9	.051		
		.78		7.8	9.8	.0088	3.0	.137	5.4	.078
		.80		7.8	9.9	.0091			5.0	.096
		.85		7.8	10.0	.0099			4.7	.072
		.90		7.8	9.9	.0061			4.8	.058
		.95		7.8	10.1	.0046			5.0	.075
R-2	F-2	.65	0.16		9.2	.0230	2.3	.113		
		.65	0.32		9.3	.0220				
		.65	0.64		8.9	.0209				
		.65	0.96		8.7	.0169				
		.65	1.28		8.6	.0120				
		.78	0.16		9.9	.0140	2.4	.131	4.8	.129
		.78	0.32		9.9	.0135				
		.78	0.64		9.8	.0117				
		.78	0.96		9.7	.0110				
		.78	1.28		9.7	.0102				
		.78	1.46		9.6	.0105				
		.90	0.16		9.9	.0065			4.9	.017
		.90	0.32		10.1	.0062				
		.90	0.50		10.0	.0062				
		.90	0.64		10.0	.0048				
		.90	1.00		9.9	.0055				
		.90	1.48		9.9	.0056				
		.55	0.90		9.1	.0270	2.4	.140		
		.60	0.96		8.8	.0300	2.5	.164	5.2	.109
		.65	0.96		8.8	.0183	2.3	.087	5.2	.105
		.70	0.96		9.0	.0037	2.6	.006	5.2	.110
		.75	0.96		9.6	.0089	2.5	.043	5.1	.112
		.78	0.96		9.7	.0095	2.5	.089	5.2	.100
		.80	0.96		9.8	.0100	2.6	.148	5.2	.098
		.85	0.96		9.6	.0110	2.6	.147	5.2	.090
		.90	0.96		9.8	.0062	2.3		5.1	.021
		.95	0.96		10.2	.0074	2.5		5.0	.084
		.60		7.8	8.2	.0299	2.3	.160	5.2	.102
		.65		7.8	8.9	.0179	2.2	.110		
		.70		7.8	9.1	.0041	2.4	.030		
		.75		7.8	9.5	.0081	2.9	.020		
		.78		7.8	9.9	.0087	3.1	.034	5.0	.098
		.80		7.8	9.8	.0103			5.1	.110
		.85		7.8	9.7	.0107			5.1	.085
		.90		7.8	9.7	.0056			5.2	.031
		.95		7.8	10.1	.0060			5.5	.049

APPENDIX A (Continued)

Rotor Conf.	Fuse. Conf.	$\bar{\Omega}$	T g	θ deg	f_b Hz	ζ_b	f_r Hz	ζ_r	f_p Hz	ζ_p
R-4	F-2	.78	0.16		9.8	.0098				
		.78	0.32		9.8	.0091	2.6	.121	5.0	.100
		.78	0.64		9.8	.0080				
		.78	0.96		9.8	.0072				
		.78	1.28		9.7	.0059				
		.78	1.44		9.7	.0052				
		.60	0.96		8.8	.0257	2.4	.154	5.2	.121
		.65	0.96		8.9	.0192	2.4	.109		
		.70	0.96		9.0	.0037	2.5	.024		
		.75	0.96		9.4	.0072	2.9	.037		
		.78	0.96		9.7	.0079	2.9	.146	5.1	.095
		.80	0.96		9.9	.0085			5.1	.089
		.85	0.96		9.9	.0097			5.4	.071
		.90	0.96		9.8	.0057			5.2	.058
		.95	0.96		10.3	.0010	2.3		5.4	.057
R-6	F-2	.78	0.16		9.7	.0143	2.5	.145	5.2	.107
		.78	0.32		9.7	.0135				
		.78	0.64		9.6	.0129				
		.78	0.96		9.5	.0113				
		.78	1.28		9.4	.0107				
		.78	1.44		9.4	.0094				
		.60	0.96		8.4	.0184	2.5	.175	5.2	.116
		.65	0.96		8.6	.0113	2.3	.081		
		.70	0.96		9.0	0	2.6	.004		
		.75	0.96		9.4	.0063	2.9	.028		
		.78	0.96		9.6	.0102	2.9	.134	5.1	.101
		.80	0.96		9.7	.0110			5.1	.098
		.85	0.96		9.7	.0121			5.3	.096
		.90	0.96		9.8	.0030			5.3	.040
		.95	0.96		10.0	.0030	2.5		5.6	.046
R-7	F-2	.78	0.16		9.5	.0127	2.6	.152	5.4	.103
		.78	0.32		9.6	.0104				
		.78	0.64		9.6	.0087				
		.78	0.96		9.6	.0076				
		.78	1.28		9.5	.0057				
		.78	1.44		9.5	.0043				
		.60	0.96		8.4	.0228	2.2	.151	5.1	.132
		.65	0.96		8.5	.0102	2.1	.077		
		.70	0.96		8.9	-.0071	2.6	-.011		
		.75	0.96		9.3	.0065	3.0	.029		
		.78	0.96		9.4	.0068	2.9	.145	5.3	.091
		.80	0.96		9.5	.0125			5.3	.085
		.85	0.96		9.6	.0172			5.2	.093
		.90	0.96		9.8	.0037			5.4	.036
		.95	0.96		10.1	-.0017			5.5	-.002

APPENDIX A (Continued)

Rotor Conf.	Fuse. Conf.	$\bar{\Omega}$	T g	θ deg	f_b Hz	ζ_b	f_r Hz	ζ_r	f_p Hz	ζ_p
R-1	F-3	.65	0.16		9.0	.0177	2.4	.120	5.0	.054
		.65	0.32		8.9	.0178				
		.65	0.64		8.6	.0162				
		.65	0.96		8.5	.0124				
		.65	1.28		8.5	.0060				
		.78	0.16		9.9	.0105	2.6	.117	5.1	.057
		.78	0.32		9.8	.0097				
		.78	0.64		9.8	.0084				
		.78	0.96		9.6	.0074				
		.78	1.28		9.5	.0070				
		.78	1.44		9.5	.0060				
		.90	0.16		9.9	.0032	2.4	.096	4.9	.028
		.90	0.32		9.9	.0006				
		.60	0.96		8.6	.0233	2.4	.148	4.8	.059
		.65	0.96		8.6	.0151	2.3	.149	4.8	.061
		.70	0.96		9.2	.0031	2.4	.007	4.7	.065
		.75	0.96		9.5	.0090	2.3	.048	4.6	.057
		.78	0.96		9.7	.0100	2.5	.104	4.7	.060
		.80	0.96		9.6	.0110	2.3	.116	4.7	.058
		.85	0.96		9.6	.0117	2.5	.095	4.7	.037
		.90	0.96		9.6	-.0015	2.3		4.9	-.001
		.95	0.96		10.3	.0030	2.3		5.0	.051
R-2	F-3	.65	0.16		8.8	.0220	2.3	.104	4.7	.067
		.65	0.32		8.9	.0210				
		.65	0.64		9.0	.0176				
		.65	0.96		8.8	.0150				
		.65	1.28		8.6	.0110				
		.78	0.16		10.0	.0100	2.7	.087	4.7	.064
		.78	0.32		10.0	.0099				
		.78	0.64		10.0	.0095				
		.78	0.96		9.9	.0093				
		.78	1.28		9.9	.0102				
		.78	1.44		9.8	.0099				
		.90	0.16		9.9	.0010			4.8	.015
		.90	0.32		10.0	-.0017				
		.90	0.64		9.9	-.0013				
		.90	0.96		10.0	-.0027				
		.90	1.28		10.0	-.0030				
		.60	0.96		9.0	.0099	2.5	.124	4.7	.054
		.65	0.96		8.8	.0143	2.4	.078	4.7	.065
		.70	0.96		9.1	0	2.5	.002	4.7	.060
		.75	0.96		9.5	.0057	2.5	.014	4.9	.064
		.78	0.96		9.7	.0090	2.4	.072	4.8	.057

APPENDIX A (Concluded)

Rotor Conf.	Fuse. Conf.	$\tilde{\Omega}$	T g	θ deg	f_b Hz	ζ_b	f_r Hz	ζ_r	f_p Hz	ζ_p
R-2	F-3	.80	0.96		9.7	.0098	2.4	.133	4.6	.064
		.85	0.96		9.7	.0109	2.5		4.6	.036
		.90	0.96		9.8	-.0021			4.9	-.005
		.95	0.96		10.3	.0114	2.3		5.2	.050
R-6	F-3	.65	0.16		8.8	.0206	2.3	.105	4.5	.069
		.65	0.32		8.9	.0194				
		.65	0.64		8.8	.0171				
		.65	0.96		8.9	.0135				
		.65	1.28		8.6	.0052				
		.78	0.16		9.7	.0127	2.5	.140	4.7	.066
		.78	0.32		9.5	.0120				
		.78	0.64		9.6	.0112				
		.78	0.96		9.6	.0098				
		.78	1.28		9.5	.0080				
		.78	1.44		9.5	.0050				
		.90	0.16		9.8	-.0007			4.9	-.001
		.90	0.32		9.9	-.0018				
		.90	0.64		9.8	-.0034				
		.90	0.96		9.8	-.0041				
		.90	1.28		9.8	-.0043				
		.60	0.96		8.9	.0192	2.3	.146	4.7	.066
		.65	0.96		8.6	.0099	2.2	.081		
		.70	0.96		9.1	-.0015	2.5	.006		
		.75	0.96		9.4	.0062	2.9	.028		
		.78	0.96		9.6	.0112	3.0	.153	4.6	.050
		.80	0.96		9.5	.0119			4.6	.059
		.85	0.96		9.4	.0080			4.6	.032
		.90	0.96		9.9	-.0043			4.9	-.009
		.95	0.96		10.2	.0045	2.4		5.2	.061

APPENDIX B

CALCULATED STABILITY CHARACTERISTICS FROM THE BASIC ANALYSIS

Rotor Conf.	Fuse. Conf.	$\bar{\Omega}$	T g	θ deg	f_b Hz	ζ_b	f_r Hz	ζ_r	f_p Hz	ζ_p
R-1	F-1	.65	0.02	0	9.3	.0030	(Isolated Rotor Analysis)			
		.65	0.54	5.5	9.3	.0281				
		.65	0.98	9.1	9.2	.0379				
		.65	1.40	12.4	9.2	.0561				
		.78	0.04	0	9.7	.0275				
		.78	0.52	4.0	9.7	.0237				
		.78	1.00	7.0	9.7	.0285				
		.78	1.46	9.5	9.6	.0386				
		.90	0.04	0	10.1	.0250				
		.90	0.56	3.5	10.1	.0205				
		.90	1.00	5.6	10.1	.0223				
		.90	1.44	7.6	10.1	.0277				
		.60	0.96	10.3	9.1	.0404				
		.70	0.98	8.1	9.4	.0337				
		.85	1.00	6.1	9.9	.0245				
		.95	1.00	5.2	10.3	.0204				
R-2	F-1	.65	0.06	0	9.3	.0292				
		.65	0.60	5.5	9.3	.0276				
		.65	1.04	9.1	9.2	.0377				
		.65	1.48	12.4	9.2	.0564				
		.78	0.06	0	9.7	.0265				
		.78	0.58	4.0	9.7	.0230				
		.78	1.08	7.0	9.7	.0281				
		.78	1.52	9.5	9.6	.0385				
		.90	0.06	0	10.1	.0240				
		.90	0.64	3.5	10.1	.0197				
		.90	1.08	5.6	10.1	.0217				
		.90	1.54	7.6	10.1	.0273				
		.60	1.02	10.3	9.1	.0403				
		.70	1.04	8.1	9.4	.0334				
		.85	1.08	6.1	9.9	.0239				
		.95	1.08	5.2	10.3	.0196				
R-4	F-1	.78	0.12	0	9.7	.0229				
		.78	0.64	4.0	9.7	.0203				
		.78	1.12	7.0	9.7	.0248				
		.78	1.54	9.5	9.6	.0336				
		.60	1.02	10.3	9.1	.0374				
		.70	1.06	8.1	9.4	.0301				
		.85	1.14	6.1	9.9	.0204				
		.95	1.20	5.2	10.3	.0159				

APPENDIX B (Continued)

Rotor Conf.	Fuse. Conf.	$\bar{\Omega}$	T g	θ deg	f_b Hz	ζ_b	f_r Hz	ζ_r	f_p Hz	ζ_p
R-6	F-1	.78	0.06	0	9.7	.0200	(Isolated Rotor Analysis)			
		.78	0.58	4.0	9.7	.0165				
		.78	1.08	7.0	9.7	.0216				
		.78	1.52	9.5	9.6	.0319				
		.60	1.02	10.3	9.1	.0341				
		.70	1.04	8.1	9.4	.0265				
		.85	1.08	6.1	9.9	.0178				
		.95	1.08	5.2	10.3	.0142				
R-7	F-1	.78	0	0	9.7	.0228				
		.78	0.40	4.0	9.7	.0156				
		.78	0.92	7.0	9.7	.0194				
		.78	1.40	9.5	9.7	.0302				
		.60	0.98	10.5	9.1	.0320				
		.70	0.98	8.4	9.4	.0254				
		.85	0.96	6.5	9.9	.0166				
		.95	0.96	5.7	10.3	.0132				
R-1	F-2	.65	0.02	0	9.3	.0342	2.0	.238	4.6	.126
		.65	0.54	5.5	9.2	.0374				
		.65	0.98	9.1	9.0	.0358	1.8	.453	4.6	.135
		.65	1.40	12.4	8.8	.0349				
		.78	0.04	0	9.7	.0231	1.9	.309	4.6	.129
		.78	0.52	4.0	9.7	.0163				
		.78	1.00	7.0	9.7	.0161	2.0	.412	4.6	.137
		.78	1.46	9.5	9.7	.0166				
		.90	0.04	0	10.1	.0122	2.0	.347	4.6	.149
		.90	0.56	3.5	10.2	.0044				
		.90	1.00	5.6	10.1	.0019	2.1	.407	4.6	.161
		.90	1.44	7.6	10.2	.0011				
		.60	0.96	10.3	9.0	.0520	2.0	.364	4.6	.134
		.70	0.98	8.1	9.3	.0158	1.9	.459	4.6	.135
		.85	1.00	6.1	9.9	.0112	2.1	.407	4.6	.143
		.95	1.00	5.2	10.5	.0025	2.1	.411	4.7	.157
R-2	F-2	.65	0.06	0	9.3	.0337	2.0	.236	4.6	.127
		.65	0.60	5.5	9.2	.0376				
		.65	1.04	9.1	9.0	.0371	1.8	.462	4.6	.135
		.65	1.48	12.4	8.8	.0366				
		.78	0.06	0	9.7	.0219	1.9	.310	4.6	.128
		.78	0.58	4.0	9.7	.0156				
		.78	1.08	7.0	9.7	.0148	2.0	.428	4.6	.137
		.78	1.52	9.5	9.6	.0151				
		.90	0.06	0	10.1	.0112	2.1	.348	4.6	.148
		.90	0.64	3.5	10.2	.0034				
		.90	1.08	5.6	10.2	.0010	2.1	.419	4.6	.161

APPENDIX B (Continued)

Rotor Conf.	Fuse. Conf.	$\bar{\Omega}$	T g	θ deg	f_b Hz	ζ_b	f_r Hz	ζ_r	f_p Hz	ζ_p
R-2	F-2	.90	1.54	7.6	10.2	.0001				
		.60	1.02	10.3	9.1	.0528	2.1	.370	4.7	.135
		.70	1.04	8.1	9.3	.0155	1.9	.474	4.6	.136
		.85	1.08	6.1	9.9	.0100	2.1	.419	4.6	.143
		.95	1.08	5.2	10.5	.0013	2.1	.423	4.7	.158
R-4	F-2	.78	0.12	0	9.7	.0196	2.0	.322	4.6	.134
		.78	0.64	4.0	9.7	.0129				
		.78	1.12	7.0	9.7	.0097	2.1	.442	4.6	.147
		.78	1.54	9.5	9.7	.0069				
		.60	1.04	10.3	9.0	.0482	2.2	.369	4.7	.138
		.65	1.04	9.1	9.0	.0335	1.9	.446	4.6	.140
		.70	1.06	8.1	9.3	.0123	2.0	.474	4.6	.141
		.85	1.14	6.1	10.0	.0054	2.3	.404	4.6	.154
		.90	1.16	5.6	10.3	.0005	2.3	.404	4.7	.164
		.95	1.20	5.2	10.5	.0031	2.3	.408	4.7	.158
R-6	F-2	.78	0.06	0	9.7	.0154	1.9	.310	4.6	.129
		.78	0.58	4.0	9.7	.0092				
		.78	1.08	7.0	9.7	.0084	2.0	.427	4.6	.138
		.78	1.52	9.5	9.6	.0089				
		.60	1.02	10.3	9.0	.0458	2.1	.372	4.7	.135
		.65	1.04	9.1	9.0	.0305	1.8	.449	4.6	.135
		.70	1.04	8.1	9.3	.0099	1.9	.467	4.6	[illegible]
		.78	1.08	7.0	9.7	.0083	2.0	.428	4.6	.138
		.85	1.08	6.1	9.9	.0038	2.1	.419	4.6	.143
		.90	1.08	5.6	10.2	-.0039	2.1	.419	4.6	.159
		.95	1.08	5.2	10.5	-.0036	2.1	.429	4.7	.157
R-7	F-2	.78	0	0	9.7	.0183	2.1	.349	4.6	.128
		.78	0.40	4.0	9.7	.0091				
		.78	0.92	7.0	9.7	.0065	2.1	.431	4.6	.135
		.78	1.40	9.5	9.7	.0054				
		.60	0.98	10.5	9.1	.0449	2.2	.328	4.7	.132
		.70	0.98	8.4	9.3	.0093	2.0	.459	4.7	.133
		.85	0.96	6.5	9.9	.0042	2.2	.413	4.6	.137
		.95	0.96	5.7	10.4	-.0046	2.1	.427	4.7	.155
R-1	F-3	.60	0.96	10.3	9.1	.0519	2.1	.329	4.7	.080
		.65	0.98	9.1	9.2	.0349	1.7	.430	4.7	.080
		.70	0.98	8.1	9.3	.0142	1.9	.435	4.6	.081
		.78	1.00	7.0	9.7	.0165	2.0	.383	4.6	.081
		.85	1.00	6.1	9.9	.0143	2.1	.376	4.6	.082
		.90	1.00	5.6	10.2	-.0034	2.1	.376	4.6	.118
		.95	1.00	5.2	10.5	.0017	2.1	.380	4.7	.105

APPENDIX B (Concluded)

Rotor Conf.	Fuse. Conf.	$\bar{\Omega}$	T g	θ deg	f_b Hz	ζ_b	f_r Hz	ζ_r	f_p Hz	ζ_p
R-2	F-3	.60	1.02	10.3	9.0	.0527	2.1	.335	4.7	.081
		.65	1.04	9.1	8.9	.0364	1.7	.438	4.7	.081
		.70	1.04	8.1	9.3	.0139	1.9	.449	4.7	.081
		.78	1.08	7.0	9.7	.0151	2.0	.399	4.6	.081
		.85	1.08	6.1	9.9	.0131	2.1	.388	4.6	.083
		.90	1.08	5.6	10.2	-.0042	2.1	.388	4.6	.118
		.95	1.08	5.2	10.5	.0002	2.1	.391	4.5	.106
R-6	F-3	.60	1.02	10.3	9.0	.0459	2.1	.338	4.7	.081
		.65	1.04	9.1	9.0	.0305	1.8	.420	4.7	.081
		.70	1.04	8.1	9.3	.0085	1.9	.441	4.7	.081
		.78	1.08	7.0	9.7	.0088	2.0	.398	4.6	.082
		.8	1.08	6.1	9.9	.0057	2.1	.388	4.6	.085
		.90	1.08	5.6	10.2	-.0084	2.1	.387	4.6	.115
		.95	1.08	5.2	10.5	-.0046	2.1	.391	4.5	.106

REFERENCES

1. Hohenemser, Kurt H.: Hingeless Rotorcraft Flight Dynamics. AGARD-AG-197, September 1974.

2. Ormiston, R. A.; and Bousman, W. G.: A Study of Stall-Induced Flap-Lag Instability of Hingeless Rotors. Preprint No. 730, American Helicopter Society, May 1973.

3. Chou, Pei Chi: Pitch-Lag Instability of Helicopter Rotors. Journal of the American Helicopter Society, Vol. 3, No. 3, July 1958 pages 30-39.

4. Huber, H. B.: Effect of Torsion-Flap-Lag Coupling on Hingeless Rotor Stability. Preprint No. 731, American Helicopter Society, May 1973.

5. Ormiston, R. A.: Concepts for Improving Hingeless Rotor Stability. Presented at the American Helicopter Society Mideast Region Symposium on Rotor Technology, Pennsylvania, August 1976.

6. Hodges, Dewey H.: An Aeromechanical Stability Analysis for Bearingless Rotor Helicopters. Journal of the American Helicopter Society, January 1979.

7. Cresap, Wesley L.; Myers, Alan W.; and Viswanathan, Sathy P.: Design and Development Tests of a Four-Bladed Light Helicopter Rotor System. Presented at the 34th Annual National Forum of the American Helicopter Society, May 1978.

8. Sadler, S. G.; and Ellis, D. B.: Documentation of Myklestad Analysis (DNAM06). Bell Helicopter Textron Report Number 299-099-608, August 1979.

9. Viswanathan, Sathy P.: Ground and Air Resonance Analyses of Multibladed Rotors. Bell Helicopter Textron Report Number 599-270-900, October 1975.

10. Hodges, D. H.; and Dowell, E. H.: Nonlinear Equations of Motion for the Elastic Bending and Torsion of Twisted Nonuniform Rotor Blades. NASA TN D-7818, December, 1974.

11. Tisdale, P. R.: Rotor Blade and Hub Static Design Loads. Bell Helicopter Textron Report Number 599-162-926, April 1975.

TABLE I. ROTOR MODEL DISTRIBUTED STRUCTURAL PROPERTIES

Outboard Station of Segment, m	Mass, kg/m	Structural Stiffness, N-m^2			Chordwise Radius of Gyration, m
		Beamwise	Chordwise	Torsion	
0.030	0.536	286.98	1434.9	860.94	0.0102
0.046	0.129	1.49	189.4	0.72	0.0083
0.061	0.129	1.49	189.4	0.72	0.0083
0.076	0.129	1.49	189.4	0.72	0.0037
0.090	0.113	1.43	130.9	0.57	0.0033
0.104	0.093	3.44	62.3	0.29	0.0029
0.140	0.077	4.88	35.3	0.14	0.0024
0.180	0.068	4.59	28.4	0.11	0.0021
0.218	0.068	4.59	28.4	0.11	0.0021
0.269	2.143	860.94	2582.8	860.94	0.0058
0.292	3.572	3443.76	11479.2	860.94	0.0158
0.333	2.322	573.96	5739.6	286.98	0.0196
0.427	0.518	17.22	430.5	14.35	0.0131
0.526	0.339	7.17	215.2	5.74	0.0145
0.602	0.339	7.17	215.2	5.74	0.0145
0.678	0.554	7.17	215.2	5.74	0.0113
0.754	0.339	7.17	215.2	5.74	0.0145
0.831	0.339	7.17	215.2	5.74	0.0145
0.907	0.339	7.17	215.2	5.74	0.0145
0.983	0.339	7.17	215.2	5.74	0.0145
1.059	0.339	7.17	215.2	5.74	0.0145
1.135	0.339	7.17	215.2	5.74	0.0145
1.212	0.411	10.04	215.2	5.74	0.0147

TABLE II. ROTOR BLADE DISCRETE STRUCTURAL PROPERTIES

Number of blades	4
Radius	1.212 m
Lock number	4.4
Solidity	.0734
Airfoil	NACA 0012
Blade chord	.0699 m
Blade twist	0 deg
Nominal rotor speed	81.7 rad/s
Aft chordwise offset of pitch link	.0356 m
Control system springrate	70.6 N-m/rad
Precone angle	2.75 deg
Radius of built-in precone	.0305 m
Radius of applied blade coning and sweep	.2692 m
Cuff weight	.135 kg
Cuff beamwise bending stiffness	115 $N\text{-}m^2$
Cuff inplane bending stiffness	344 $N\text{-}m^2$
Cuff torsional stiffness	201 $N\text{-}m^2$
Shear restraint radial station	.0610 m
Shear restraint inplane spring rate	59543 N/m
Flat pitch inplane damper nose-down inclination	11 deg

TABLE III. MODEL SCALE FACTORS

Item	Units	Scale Factor (a)
Length	m	5.0
Weight	N	125.0
Structural stiffness	$N-m^2$	3125.0
Angular velocity	rad/s	0.447
Linear velocity	m/s	2.236
Force	N	125.0
Moment	N-m	625.0
Power	N-m/s	279.5
Froude number		1.0
Rotor Lock number		1.0
Structural frequency ratio		1.0

[a]Ratio of full scale to model.

TABLE IV. ROTOR CONFIGURATION PARAMETRIC VALUES

Conf No.	β_b deg	γ_b deg	tan ϕ	r_{PL} cm
R-1	0	0	.330	3.56
R-2	1.5	0	.330	3.56
R-4	1.5	2	.330	3.56
R-6	1.5	0	.246	3 56
R-7	1.5	0	.246	4.83

TABLE V. ROTOR-OFF FUSELAGE PARAMETRIC VALUES FOR CONFIGURATION F-2

Item	Value
Mass moment of inertia in pitch about the c.g.	3.745 $N \cdot m \cdot s^2$
Mass moment of inertia in roll about the c.g.	1.009 $N \cdot m \cdot s^2$
Undamped natural frequency in pitch	4.9 Hz
Undamped natural frequency in roll	2.4 Hz
Height of rotor above gimbal	.4153 m
Height of c.g. above gimbal	.0127 m
Fuselage weight	289 N
Damping ratio in pitch	.115[a]
Damping ratio in roll	.065[a]

[a]For configuration F-3, the damping levels were equal respectively to one-half of the above values. All other characteristics were the same for configurations F-2 and F-3.

TABLE VI. CALCULATED INPLANE STRUCTURAL DAMPING RATIOS FOR CONFIGURATIONS R-1, R-2, AND R-4

$\bar{\Omega}$	θ	T_g	Cuff Index Angle Deg	ζ_s [a]	
				DNAM06	ARAM06
0.65	0	0.02	-11.0	0.0293	0.0294
	5.5	0.54	-5.5	0.0292	0.0293
	9.1	0.98	-1.9	0.0287	0.0288
	12.4	1.40	1.4	0.0281	0.0281
0.78	0	0.04	-11.0	0.0262	0.0263
	4.0	0.52	-7.0	0.0262	0.0263
	7.0	1.00	-4.0	0.0260	0.0261
	9.5	1.46	-1.5	0.0258	0.0258
0.90	0	0.04	-11.0	0.0234	--
	3.5	0.56	-7.5	0.0234	--
	5.6	1.00	-5.4	0.0234	--
	7.6	1.44	-3.4	0.0232	--
0.60	10.3	0.96	-0.7	0.0296	0.0296
0.70	8.1	0.98	-2.9	0.0278	0.0278
0.85	6.1	1.00	-4.9	0.0245	0.0246
0.95	5.2	1.00	-5.8	0.0222	0.0224

[a] Values tabulated correspond to a loss tangent of 0.33.

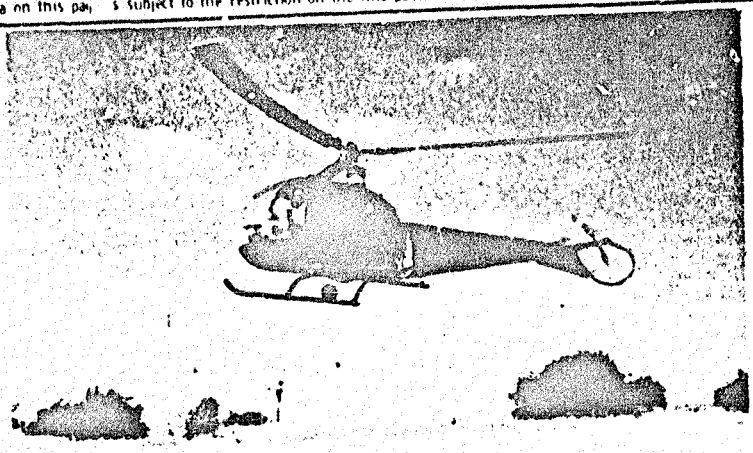

Figure 1. Three-bladed Hingeless Flexbeam Rotor on Model 47 Ranger.

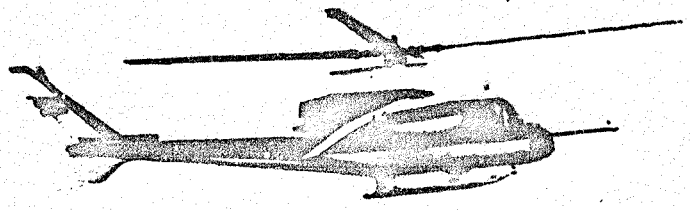

Figure 2. Four-bladed Stiff-inplane Rotor on the UH-1 Helicopter.

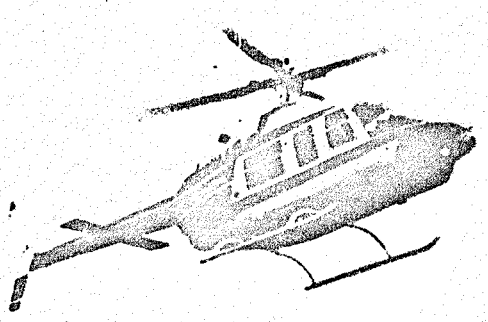

Figure 3. Model 654 Rotor on the 206L Helicopter.

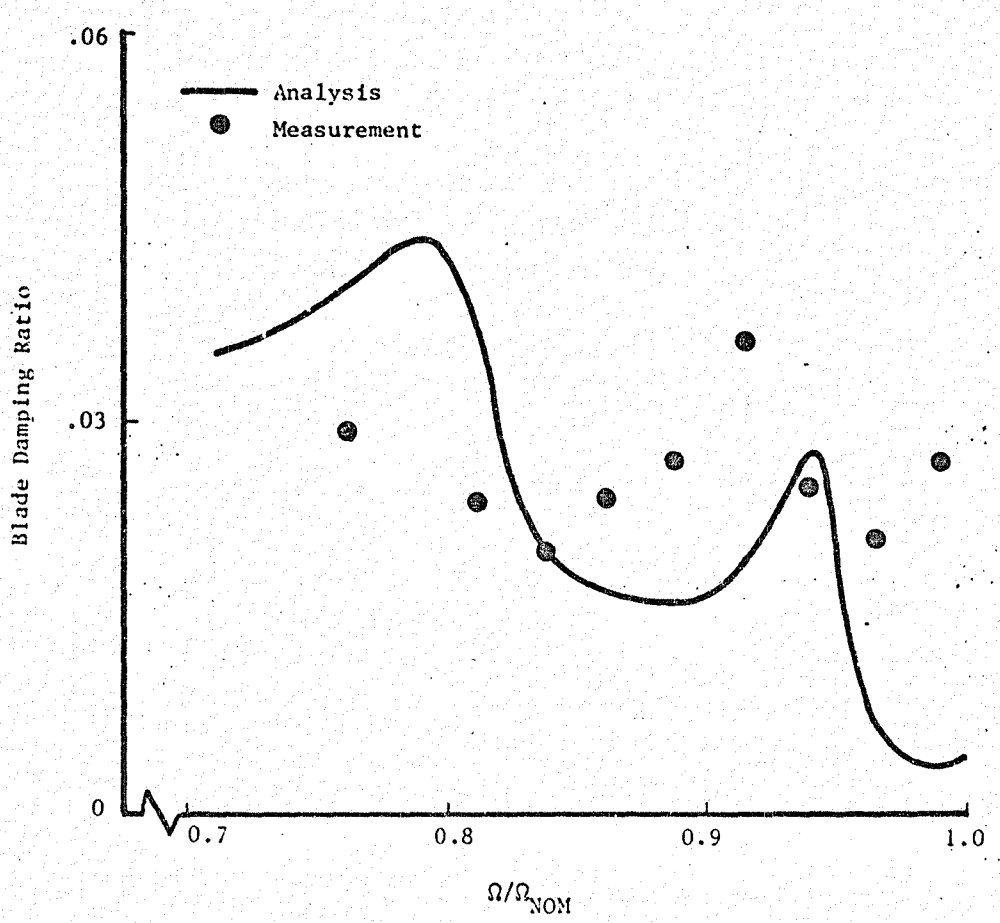

Figure 4. Inplane Damping Correlation from Ground Resonance Study of the M654 Rotor.

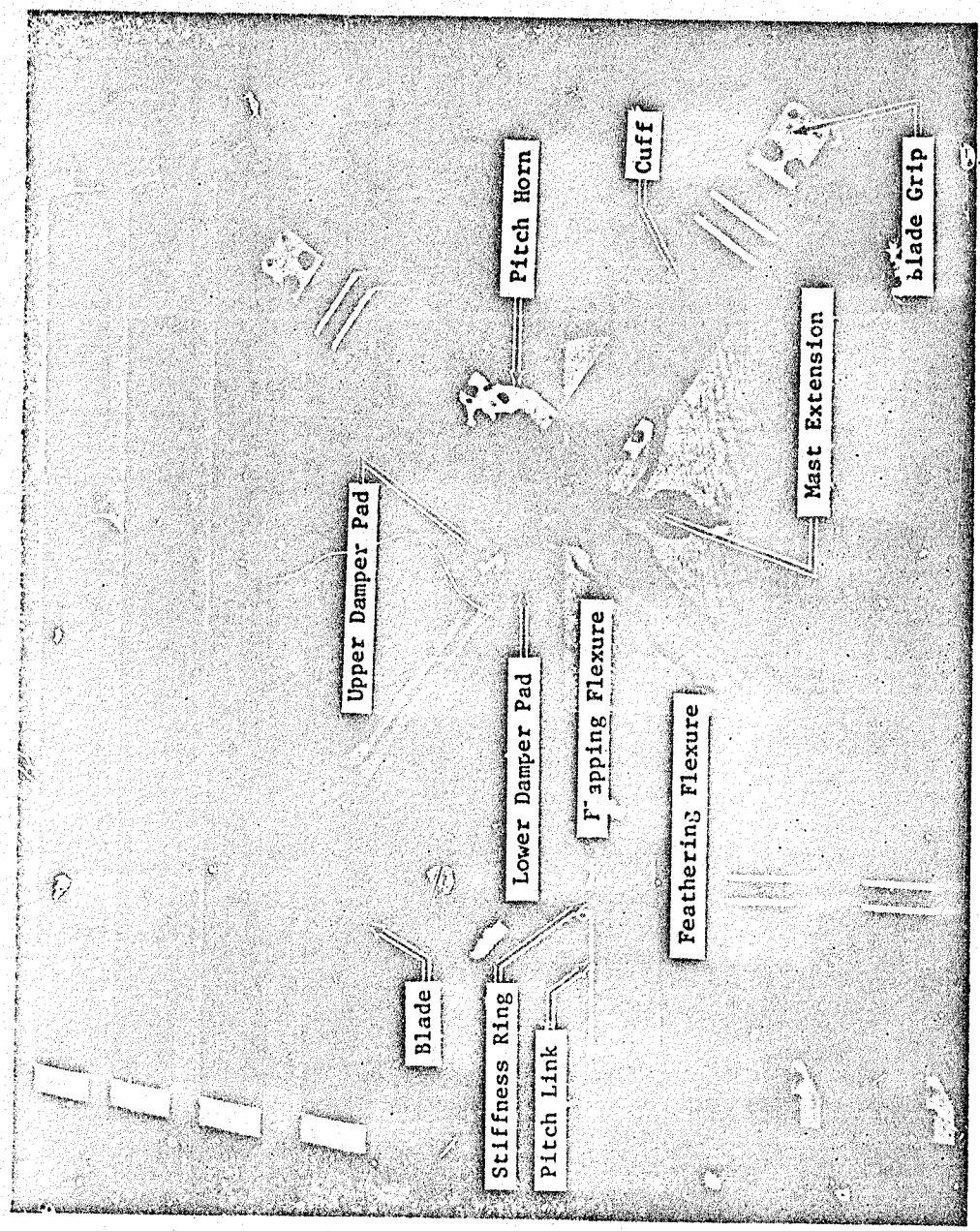

Figure 5a. Bearingless Rotor Model Hardware.

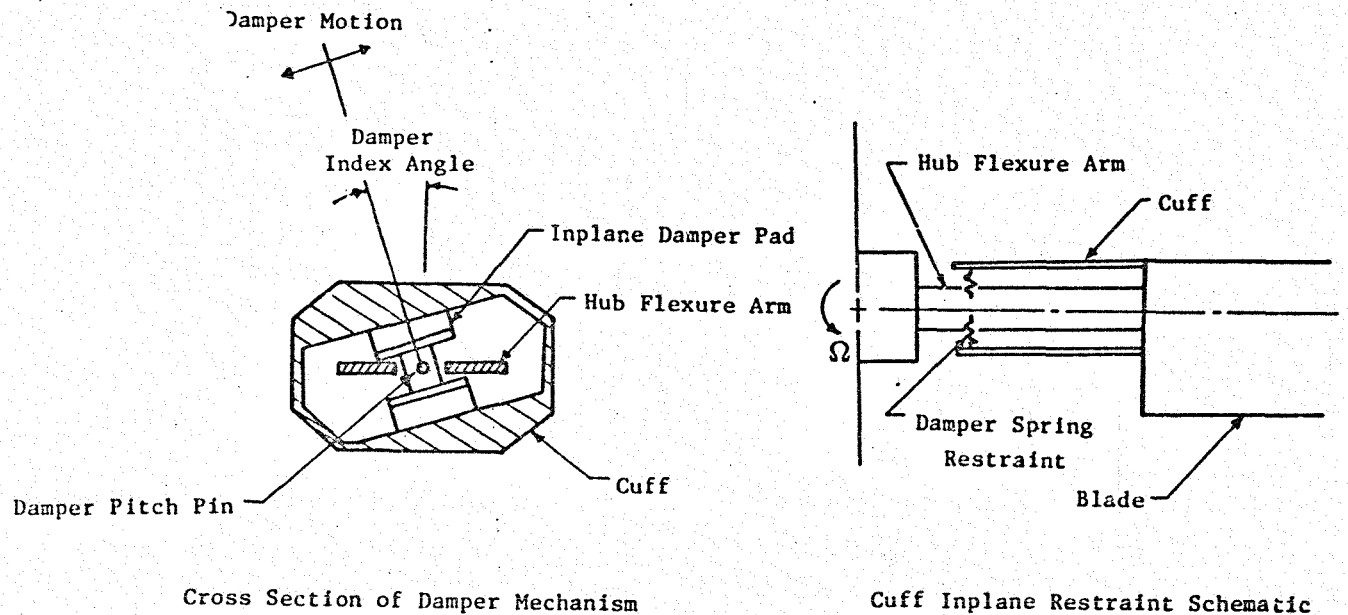

Cross Section of Damper Mechanism

Cuff Inplane Restraint Schematic

Figure 5b. Illustration of Model Shear Restraint Mechanism.

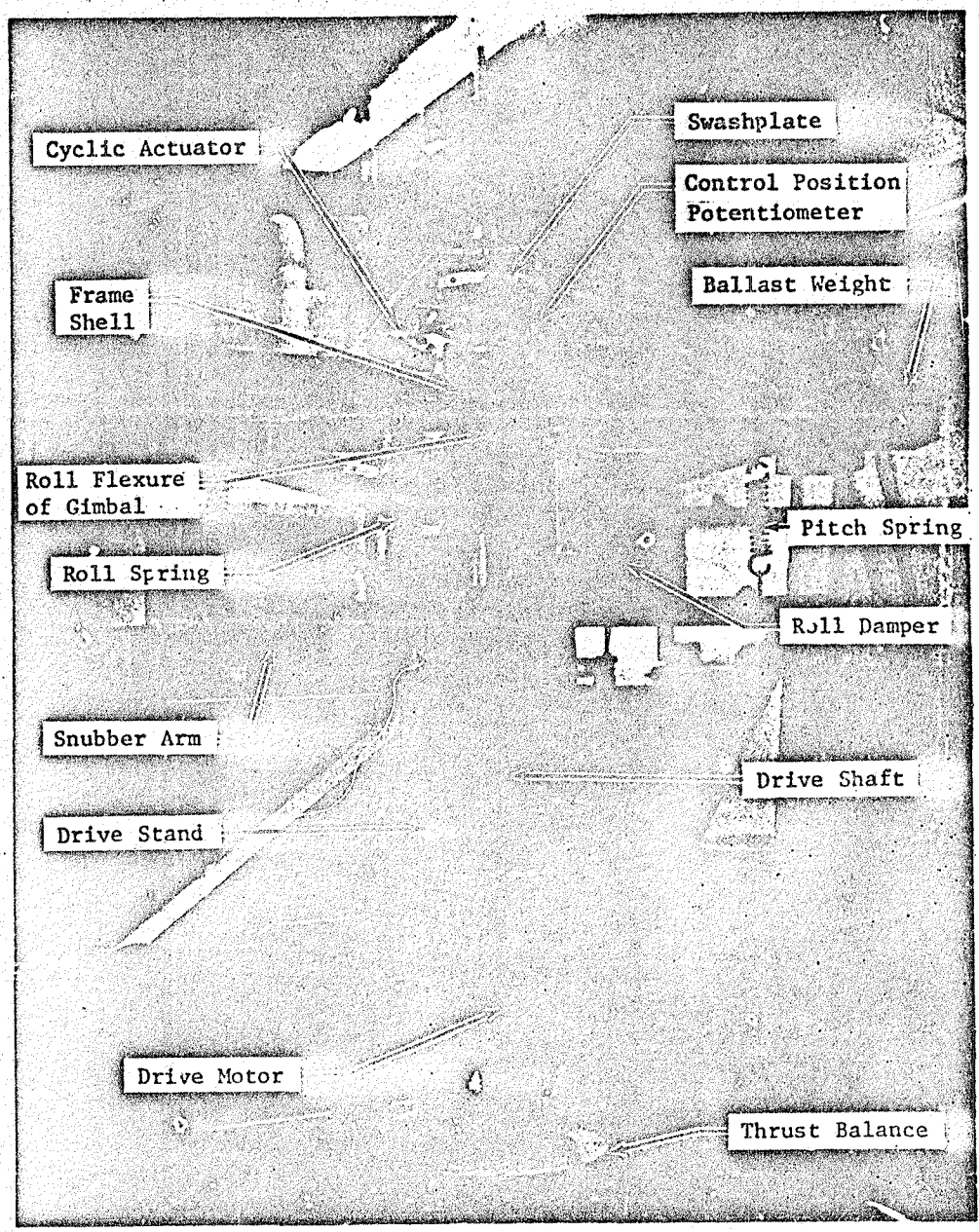

Figure 6. Detailed View of Model Fuselage.

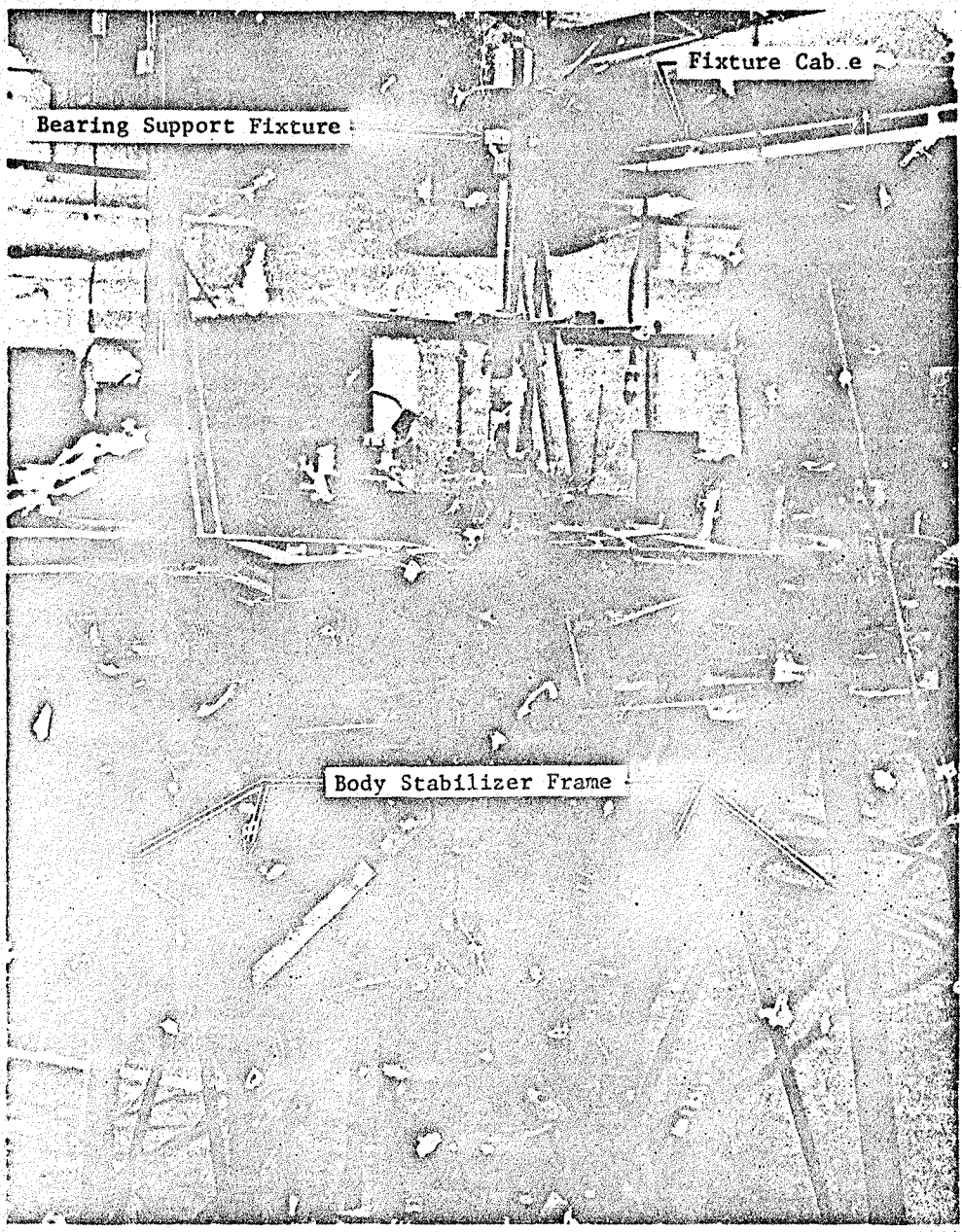

Figure 7. Isolated Rotor Test Stand Modifications.

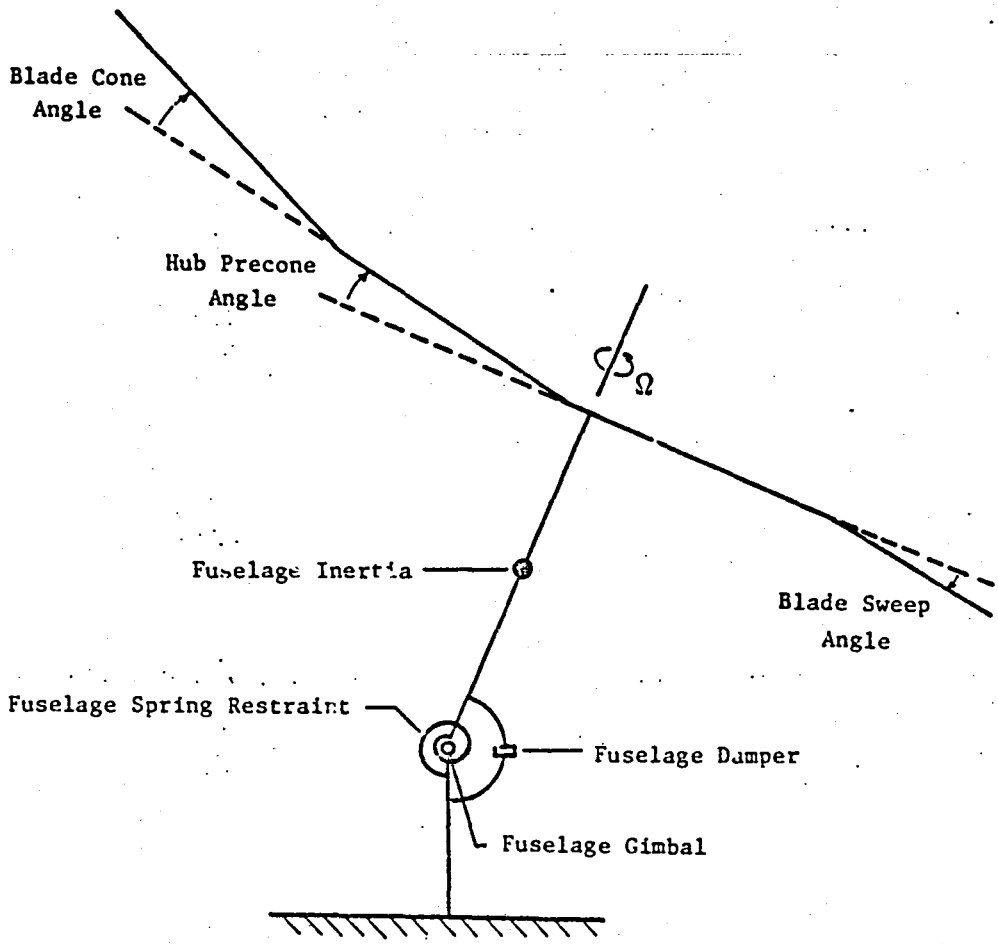

Fixed-system representation is the same for pitch and roll motions.

Figure 8. Analytical Representations in Programs ARAM06 and DRAV21TF.

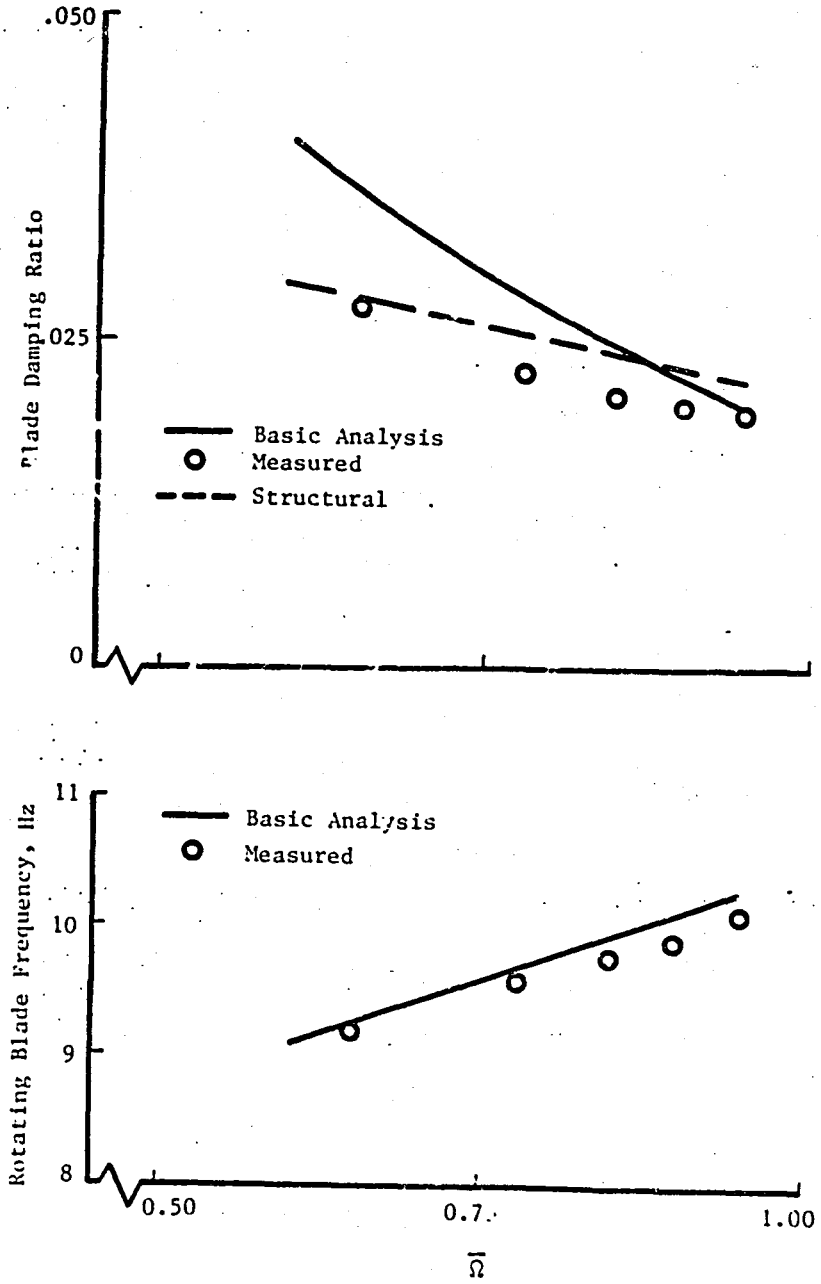

Figure 9. Inplane Damping and Frequency Correlation for Isolated Rotor Configuration R-1 (T = 1g).

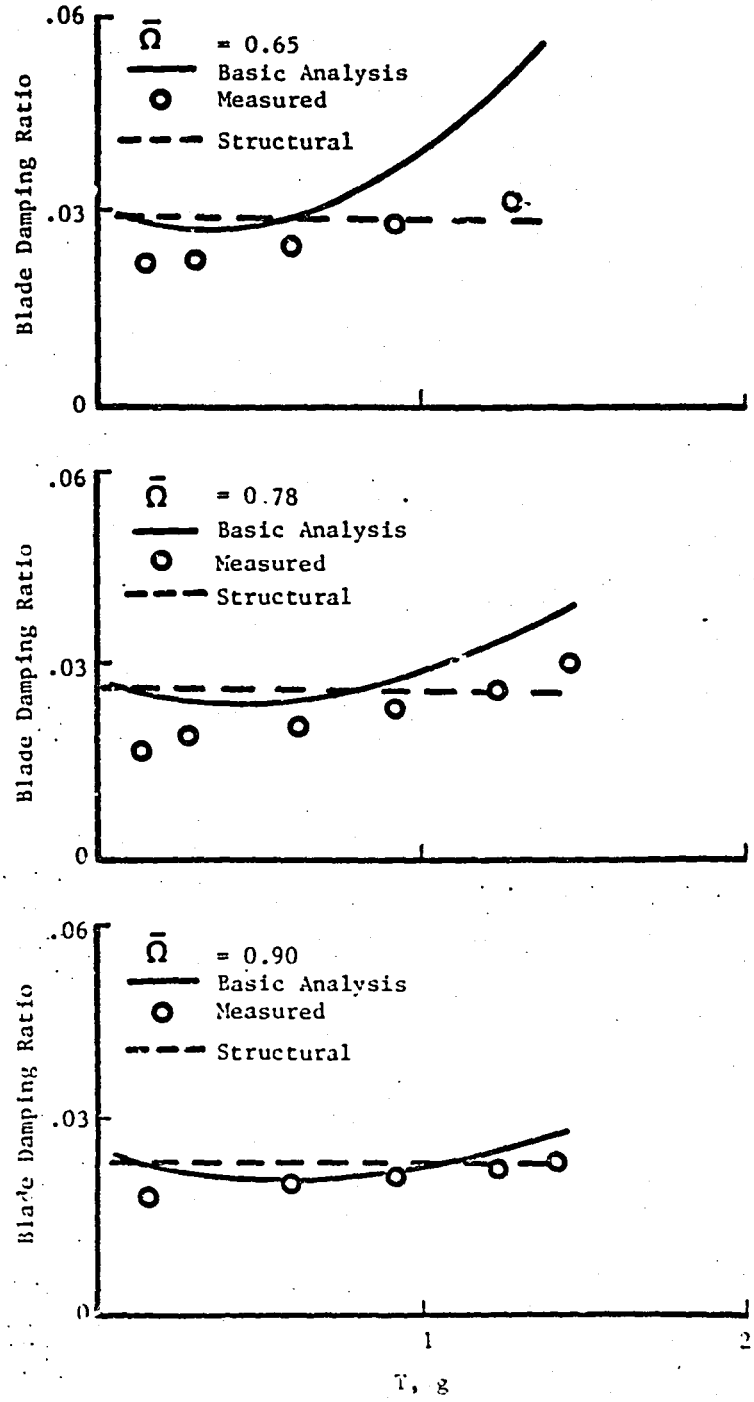

Figure 10. Inplane Damping Variations With Thrust for Isolated Rotor Configuration R-1.

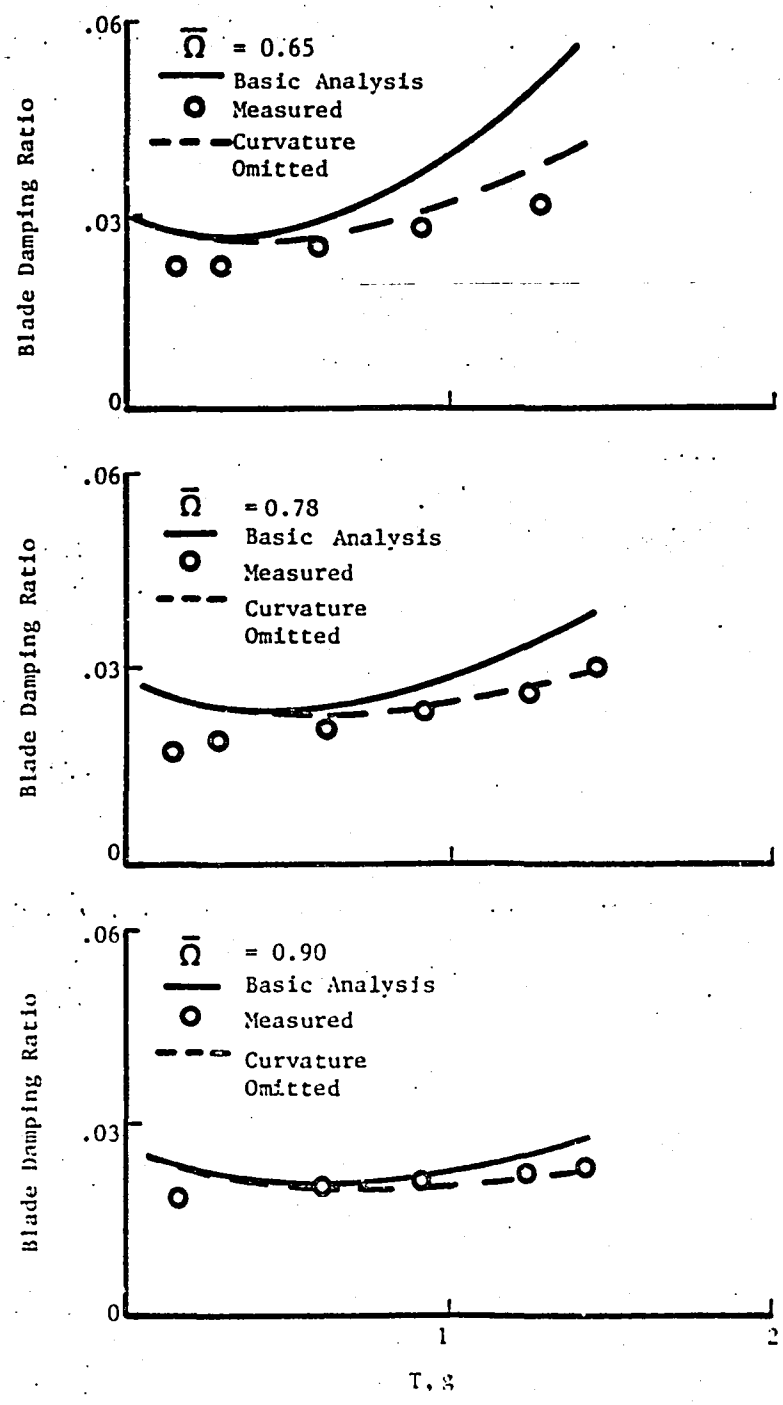

Figure 11. Bending Curvature Effects on Inplane Damping Predictions For Isolated Rotor Configuration R-1.

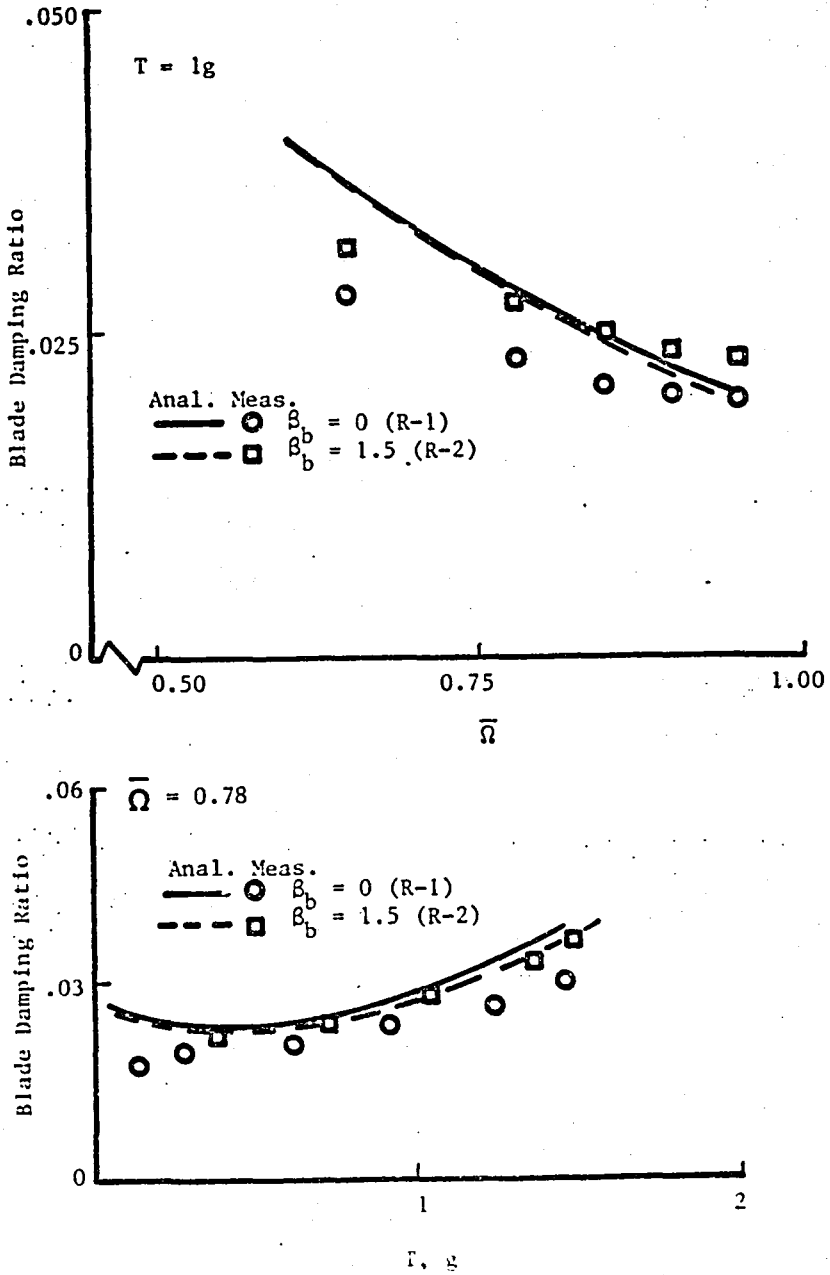

Figure 12. Variation of Inplane Damping With Blade Coning Angle, For Isolated Rotor.

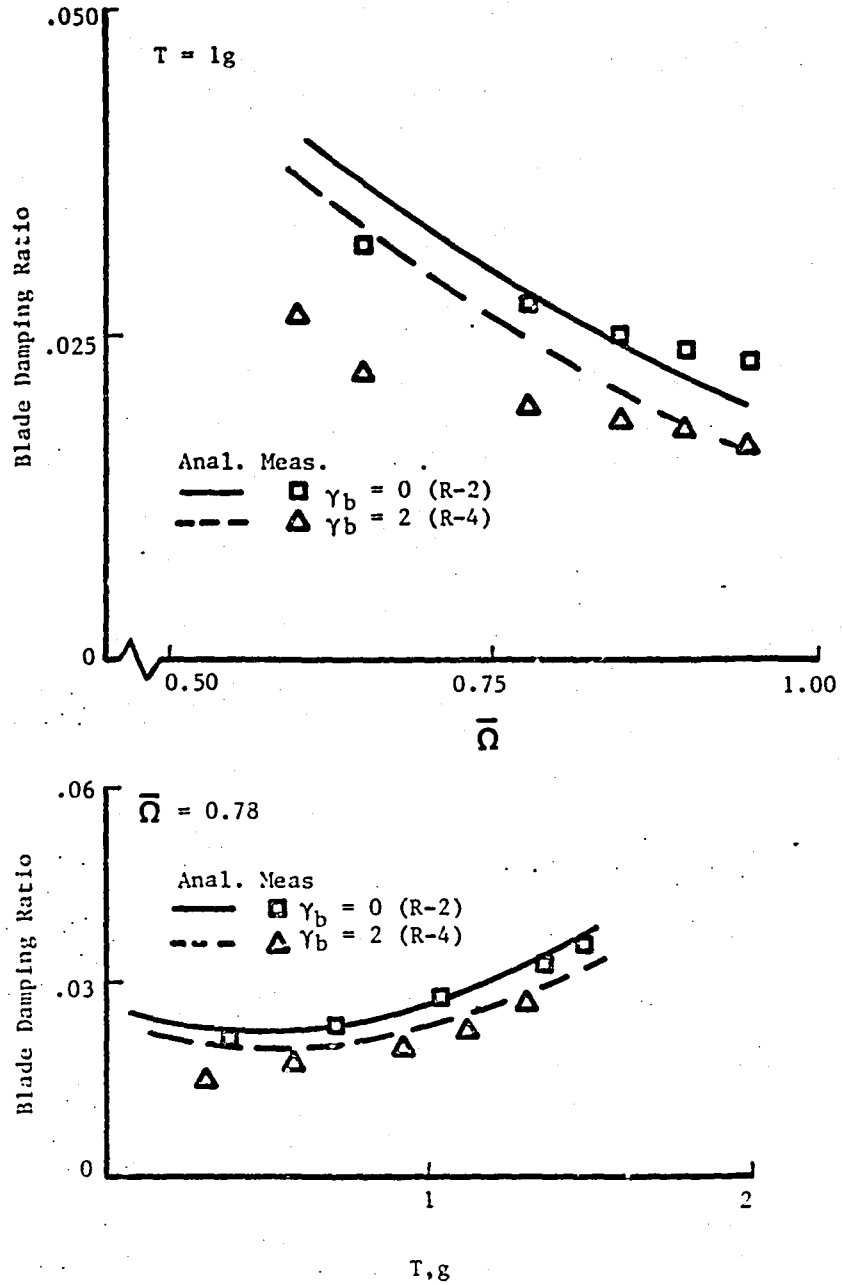

Figure 13. Variation of Inplane Damping With Blade Sweep Angle for Isolated Rotor.

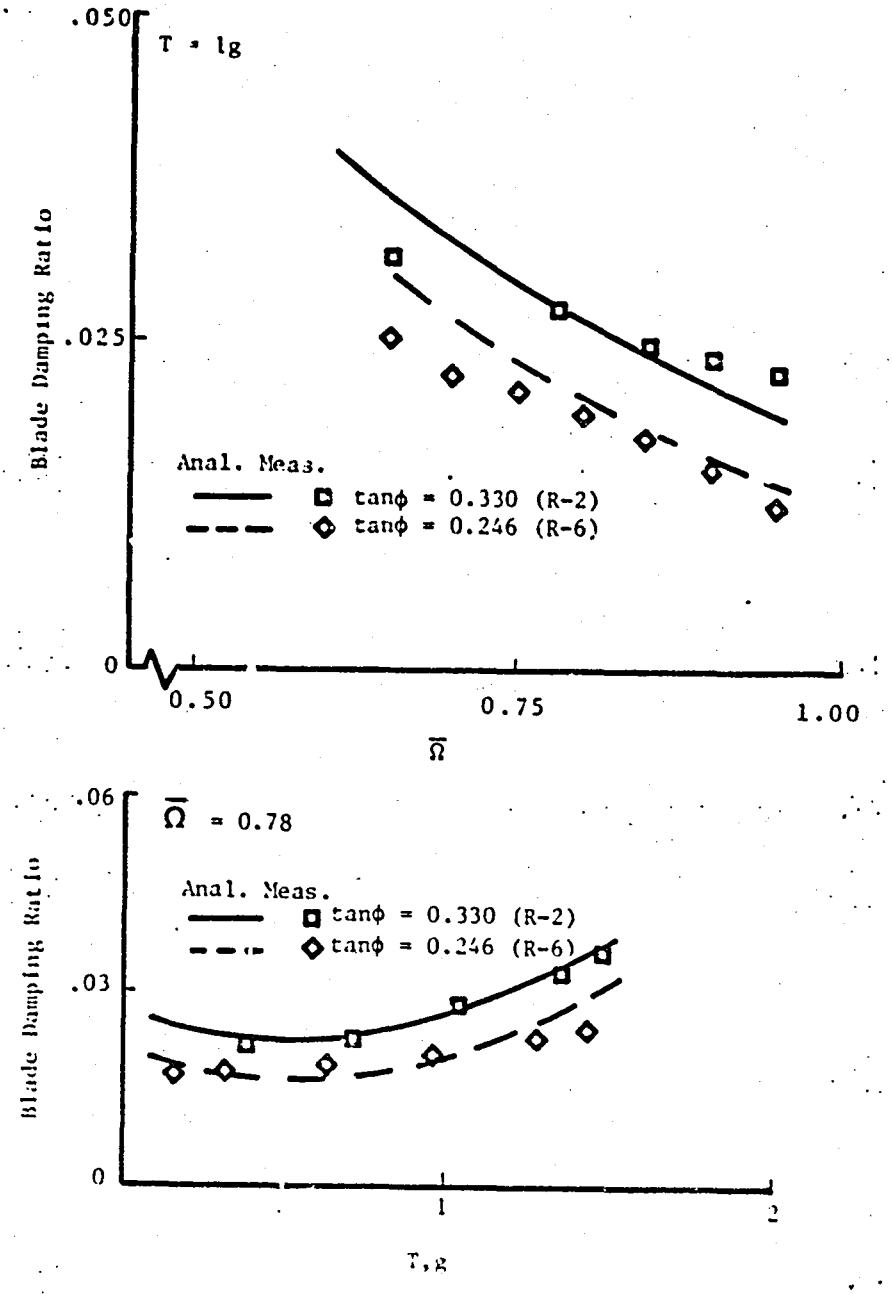

Figure 14. Variation of Inplane Damping With Hub Structural Damping for Isolated Rotor.

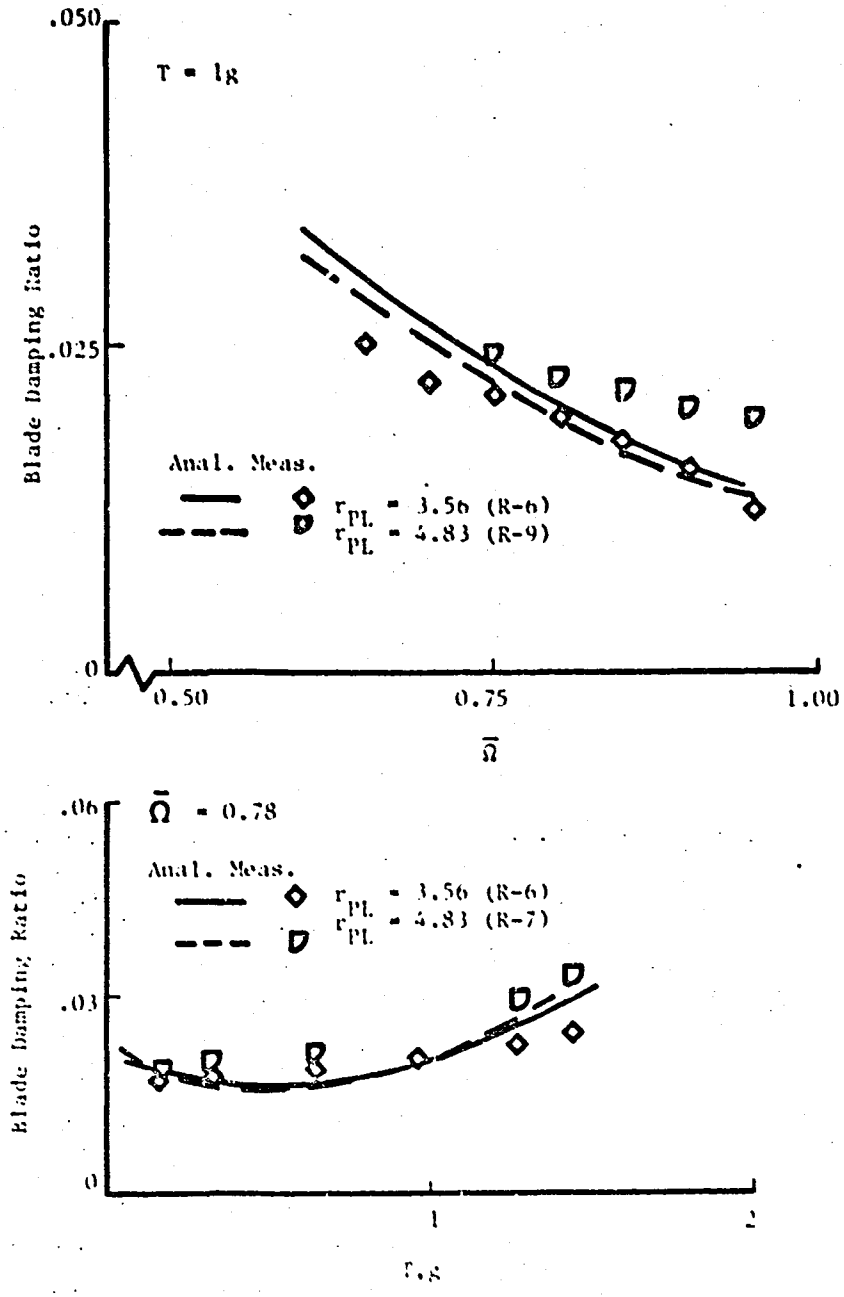

Figure 15. Variation of Blade Inplane Damping With Pitch Link Location for Isolated Rotor.

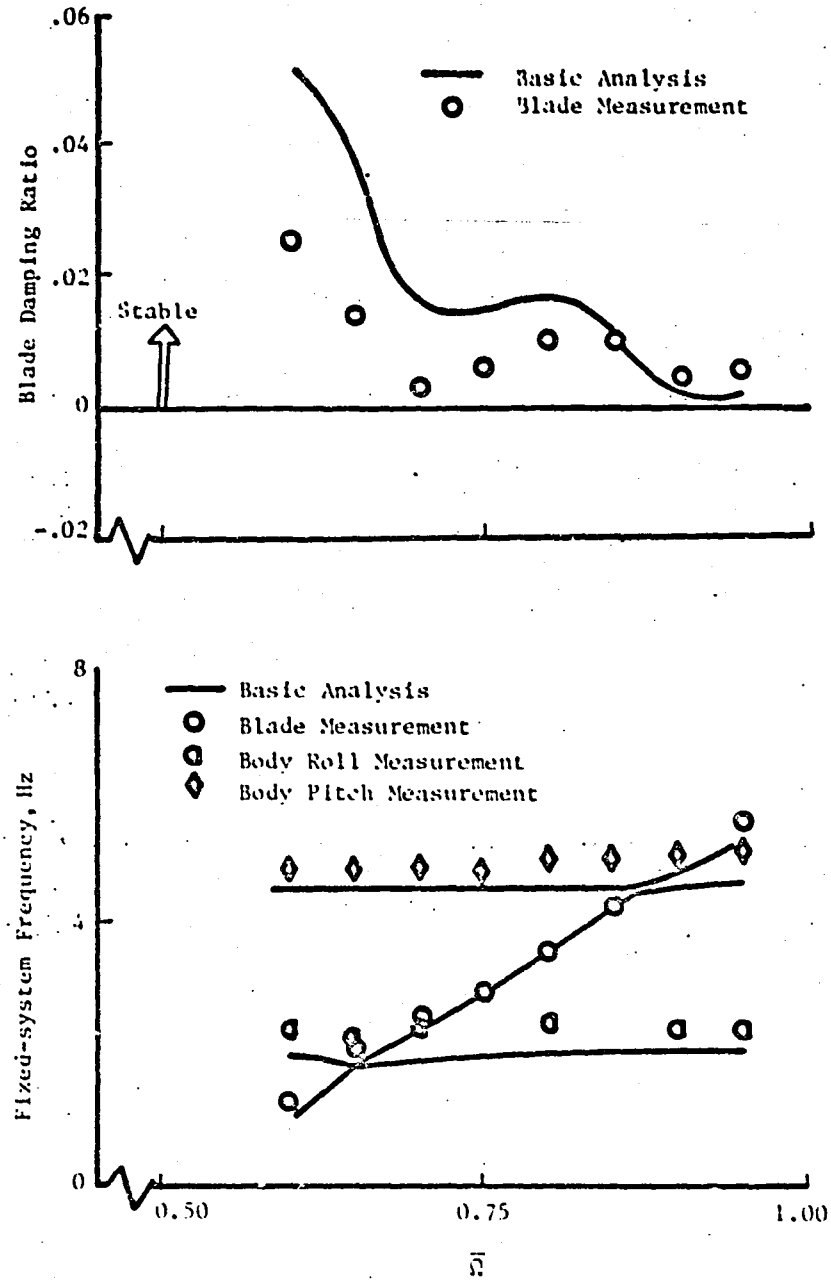

Figure 16. Inplane Damping and System Frequency Correlation For Configuration R-1/F-2 (F = 1g).

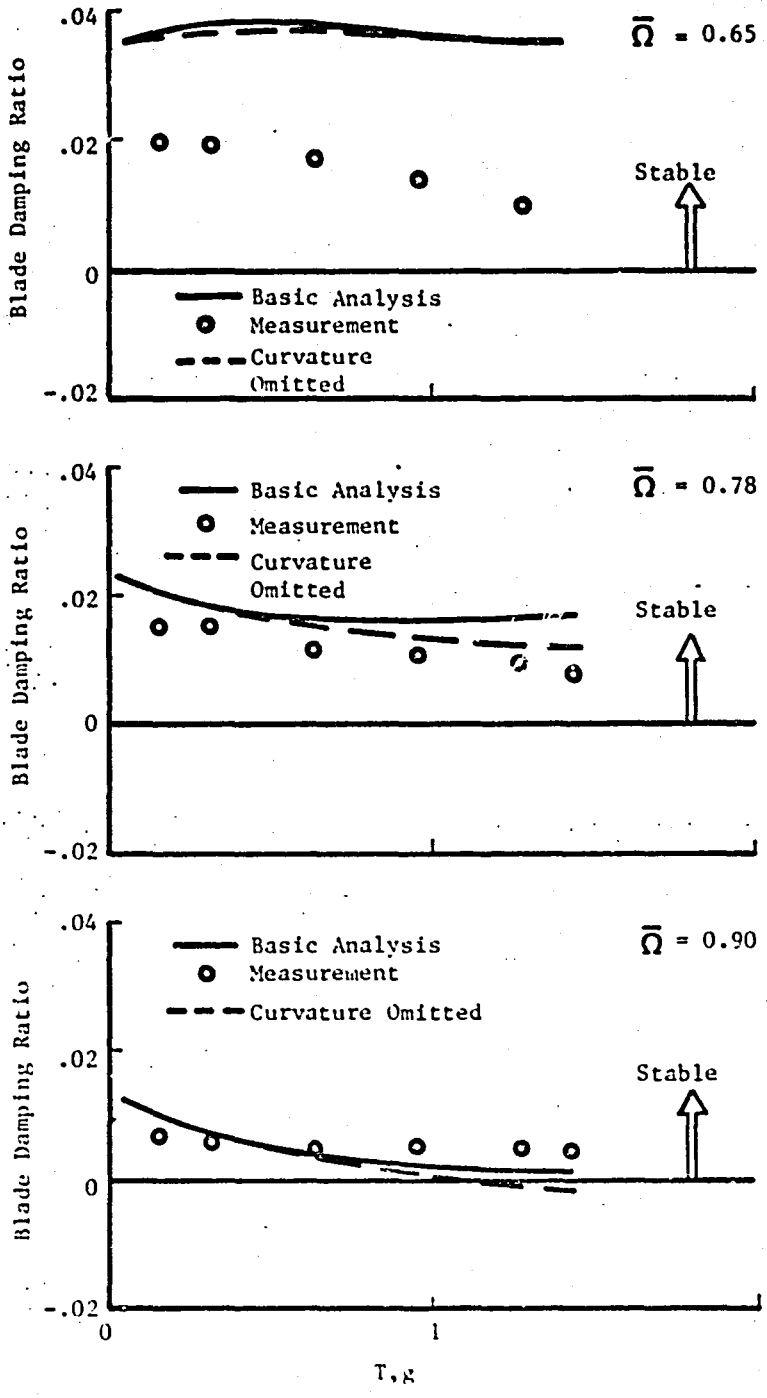

Figure 17. Bending Curvature Effects on Inplane Damping Predictions for Configuration R-1/F-2.

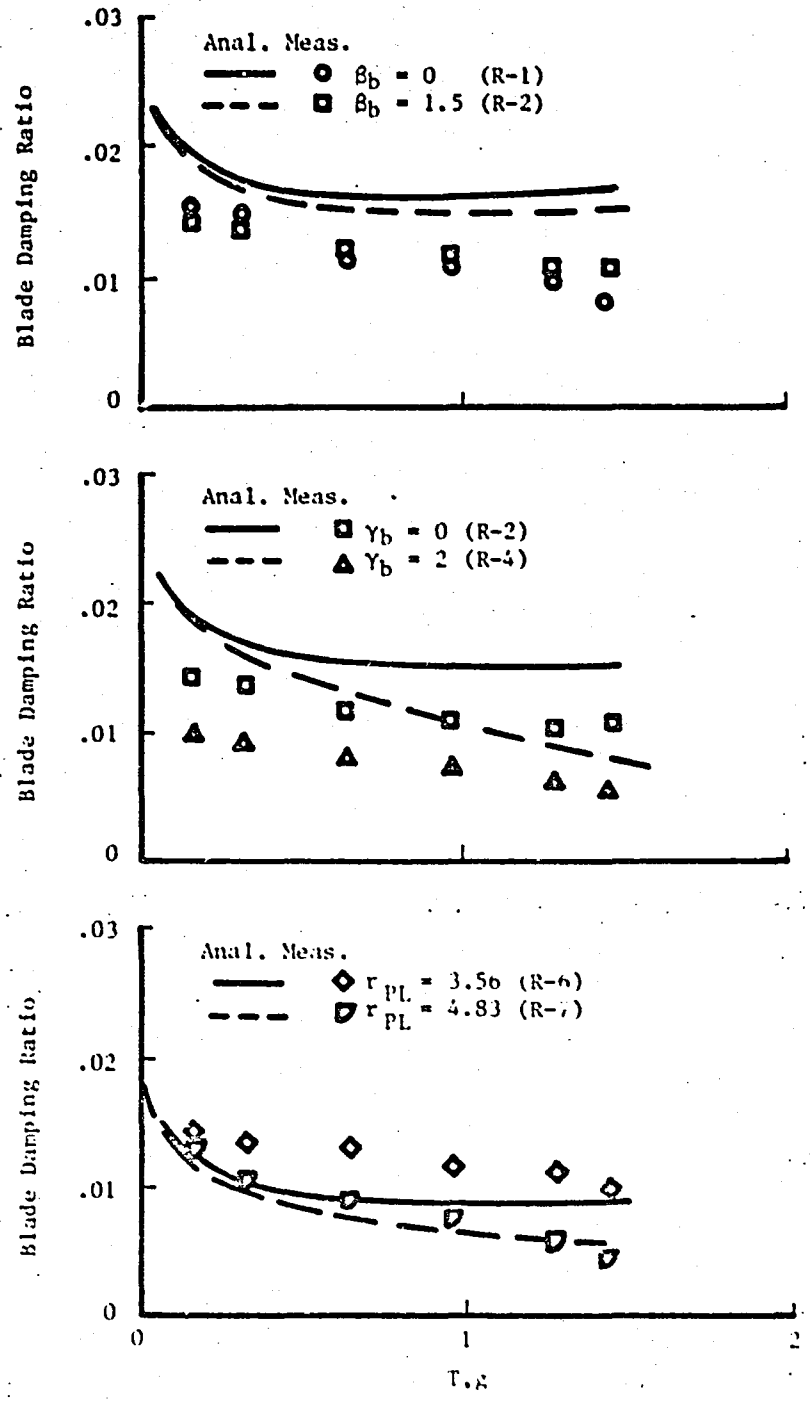

Figure 18. Variation of Inplane Damping With Blade Coning, Sweep and Pitch Link Location for Fuselage F-2 ($\bar{C}$ = 0.78).

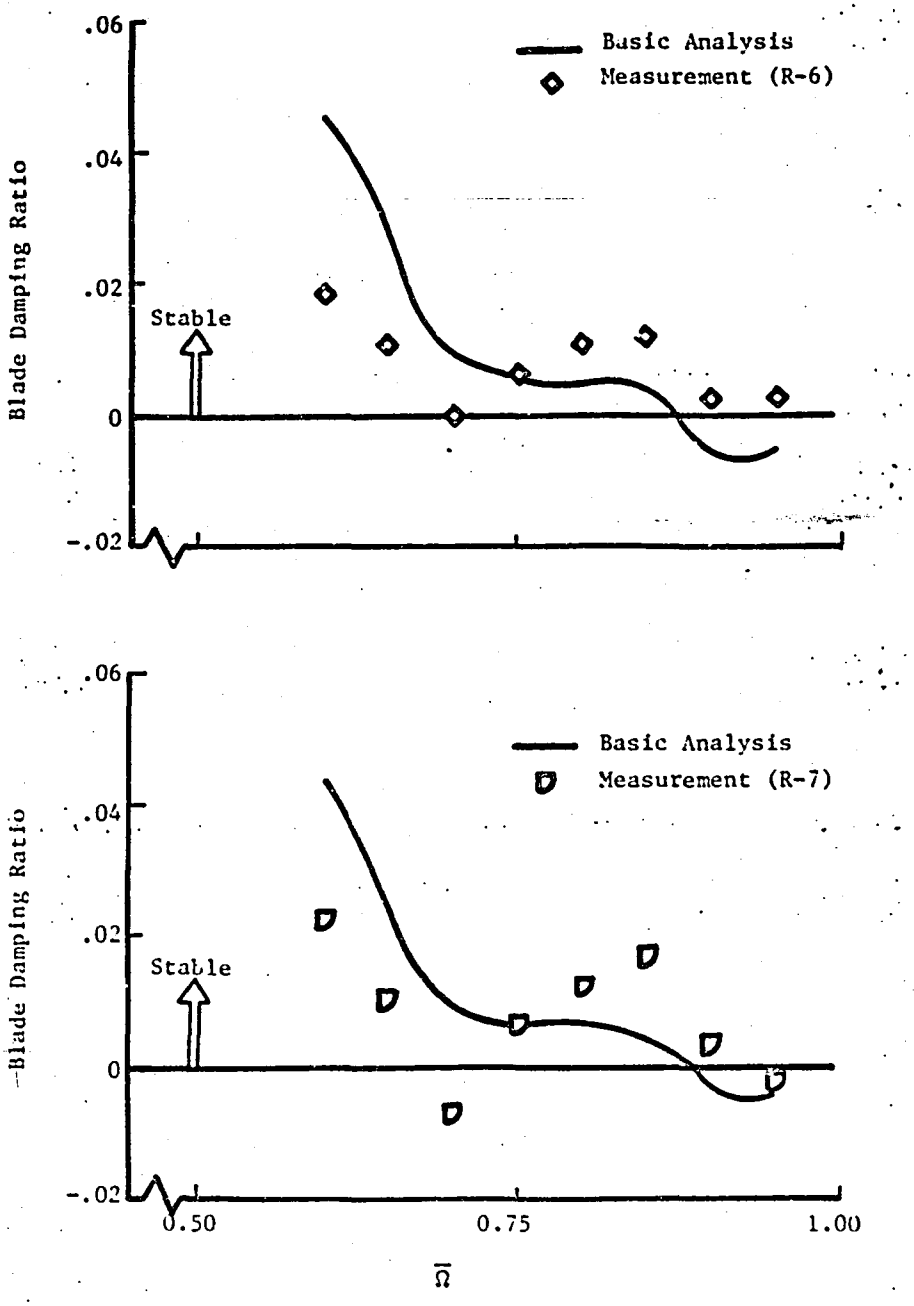

Figure 19. Minimum Stability Correlation for Fuselage F-2 (T = 1g).

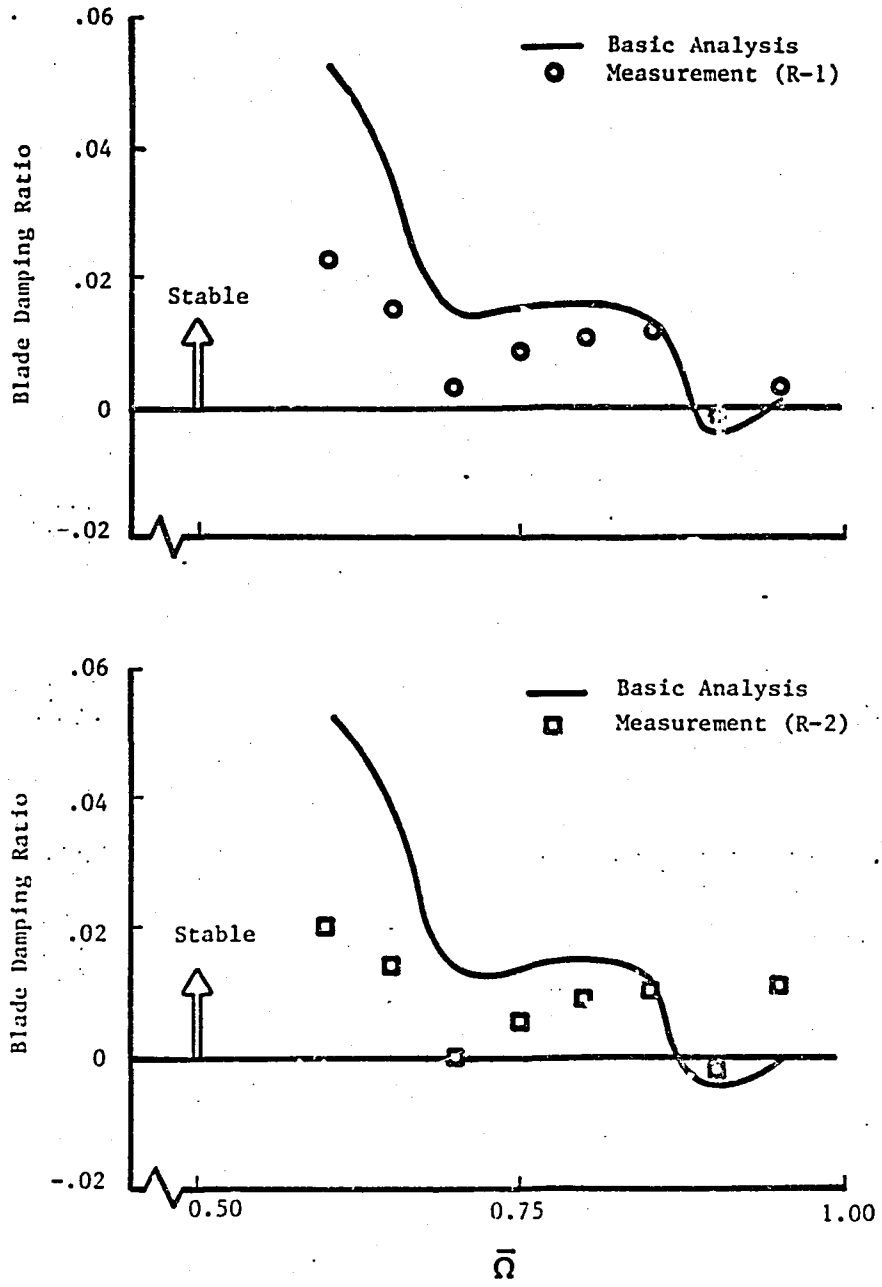

Figure 20. Correlation of Instability Conditions For Fuselage F-3 (T = 1g).

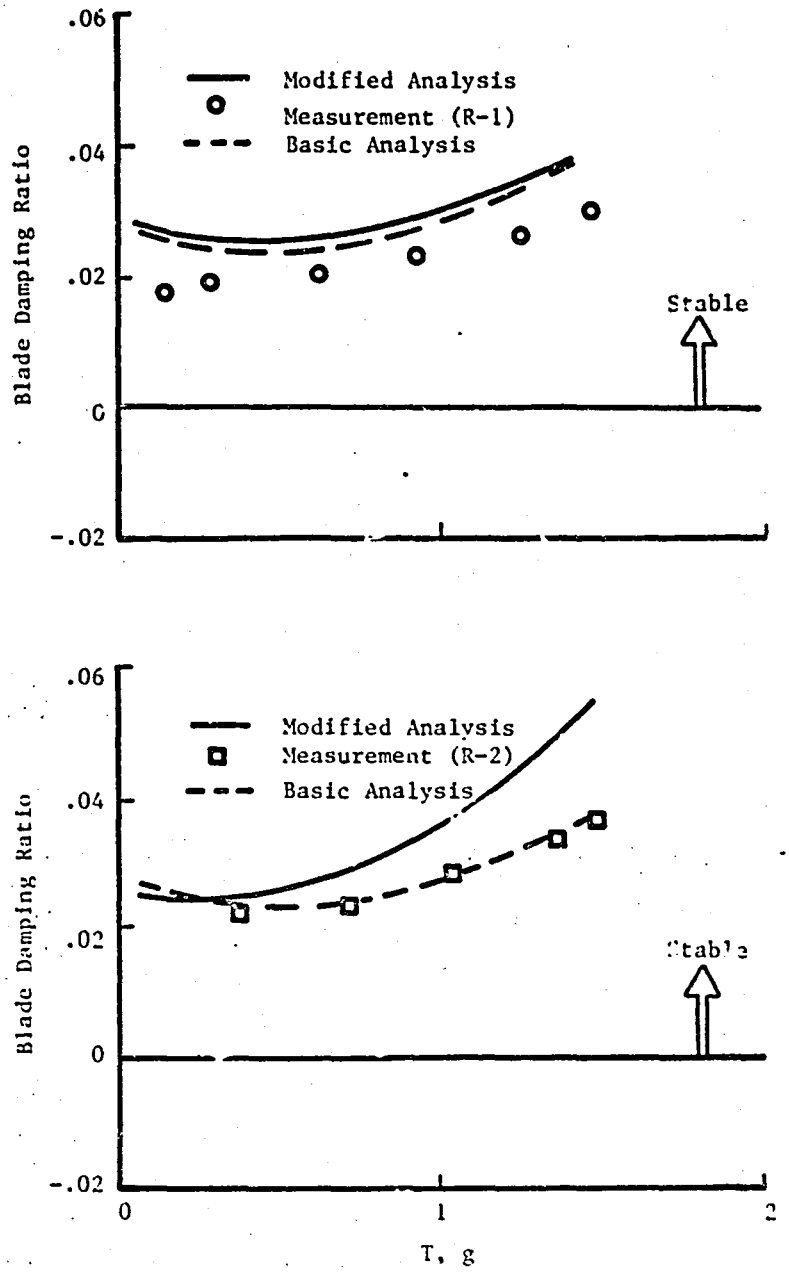

Figure 21. Inplane Damping Correlation Using the Modified (Equilibrium) Modal Analysis for Isolated Rotor ($\bar{\Omega}$ = 0.78).

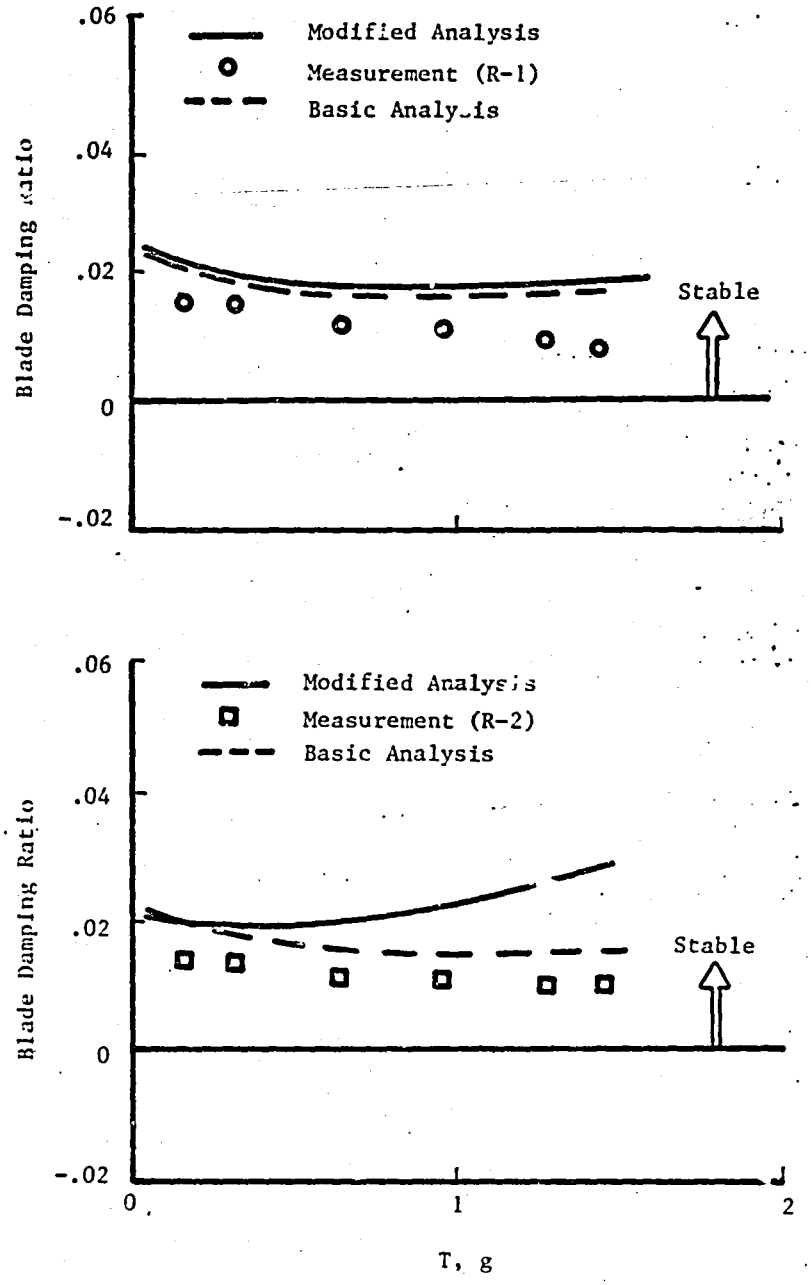

Figure 22. Inplane Damping Correlation Using the Modified (Equilibrium) Modal Analysis for Fuselage F-2 ($\bar{\Omega}$ = 0.78).

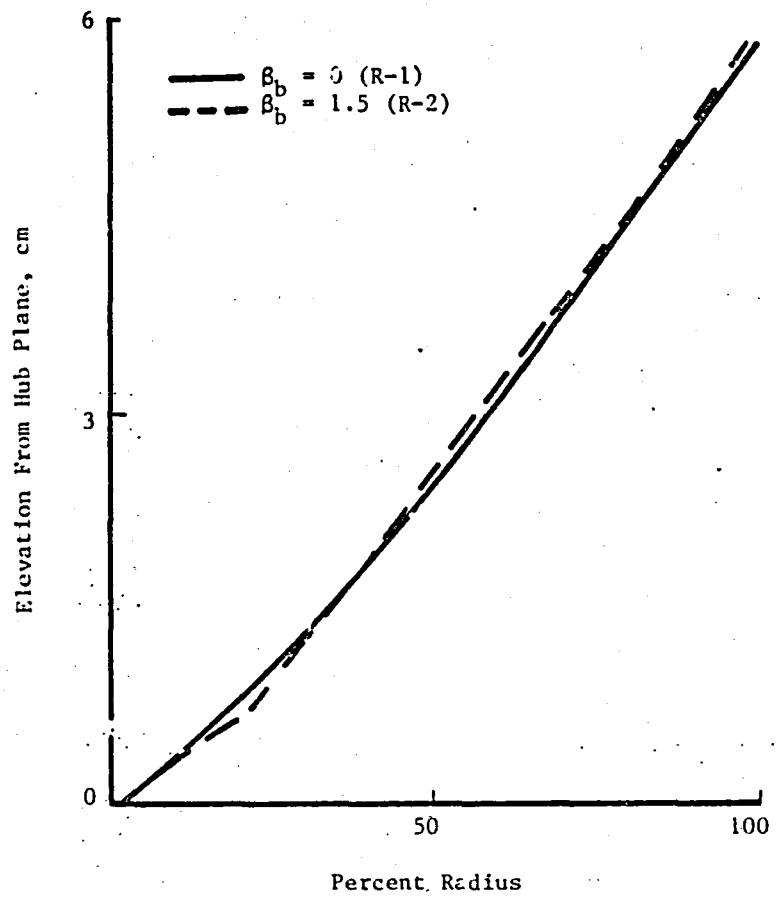

Figure 23. Effect of Blade Coning on Comp.. ! Equilibrium Position ($\bar{\Omega}$ = 0.78, T = 1.46g).

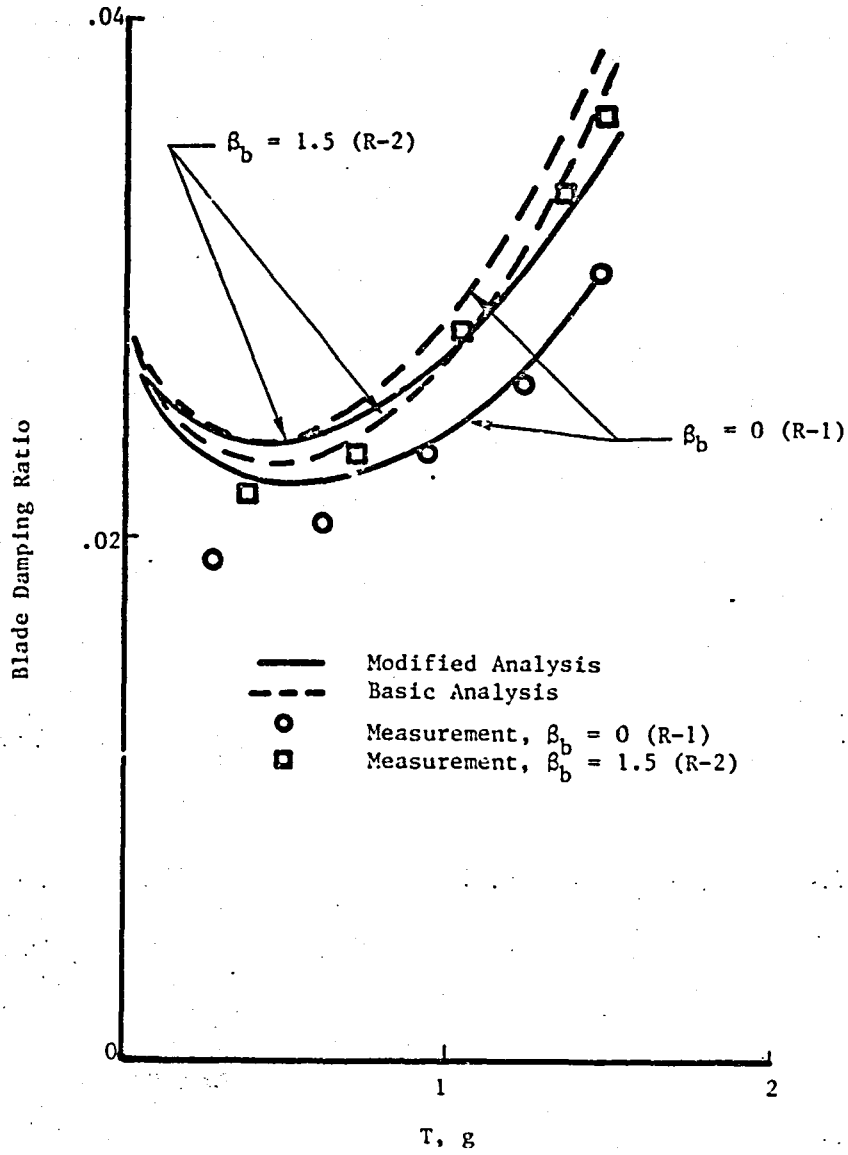

Figure 24. Damping Correlation With Blade Coning Using the Modified (Transformation) Analysis For Isolated Rotor ($\bar{\Omega}$ = 0.78).

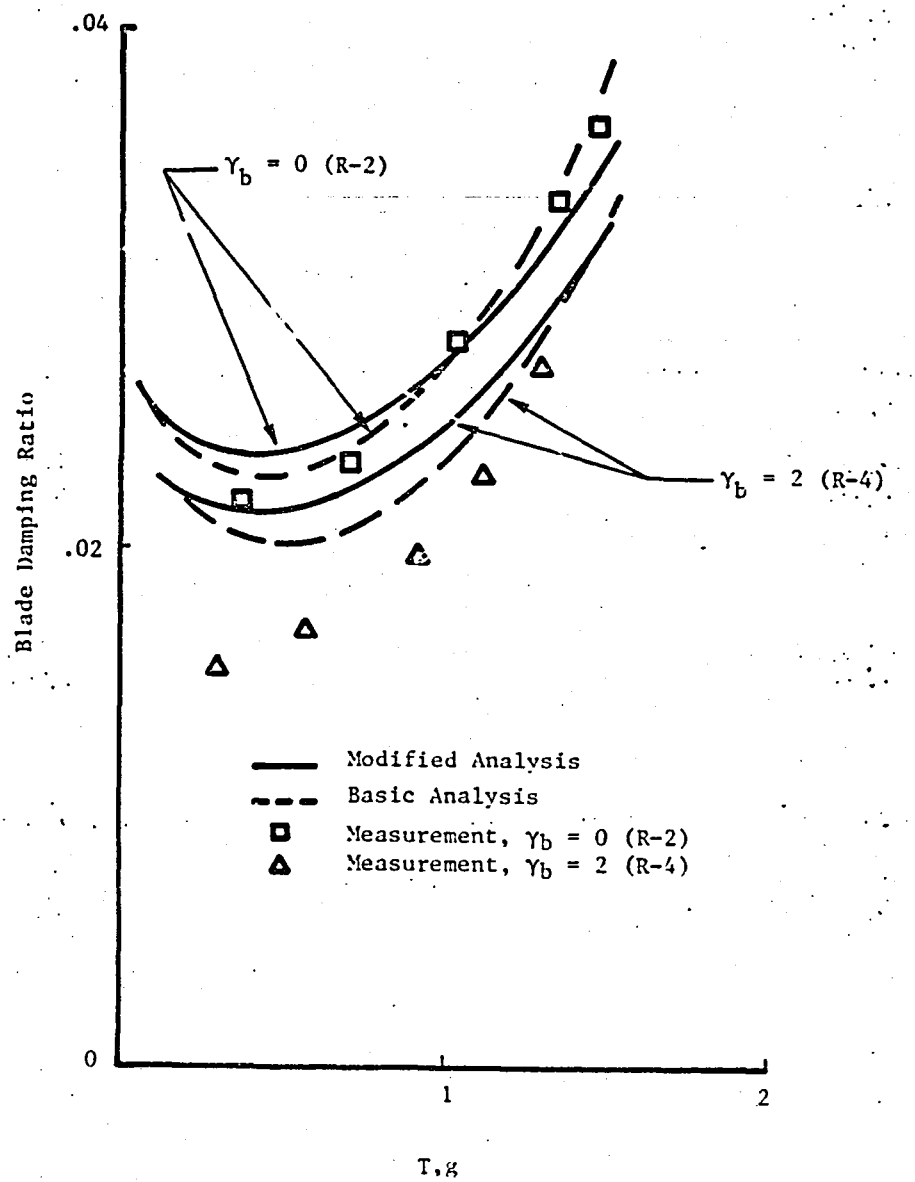

Figure 25. Damping Correlation With Blade Sweep Using the Modified (Transformation) Analysis for Isolated Rotor ($\bar{\Omega}$ = 0.78).

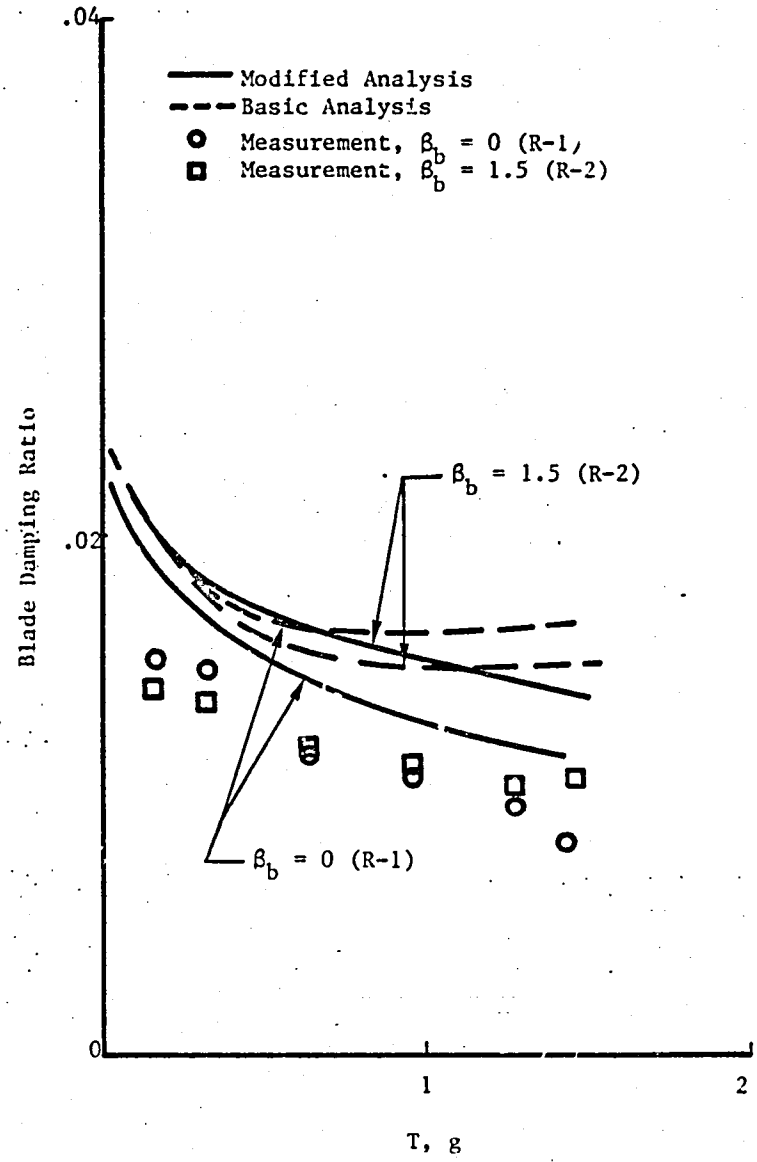

Figure 26. Damping Correlation With Blade Coning Using the Modified (Transformation) Analysis for Fuselage F-2 ($\bar{\Omega}$ = 0.78).

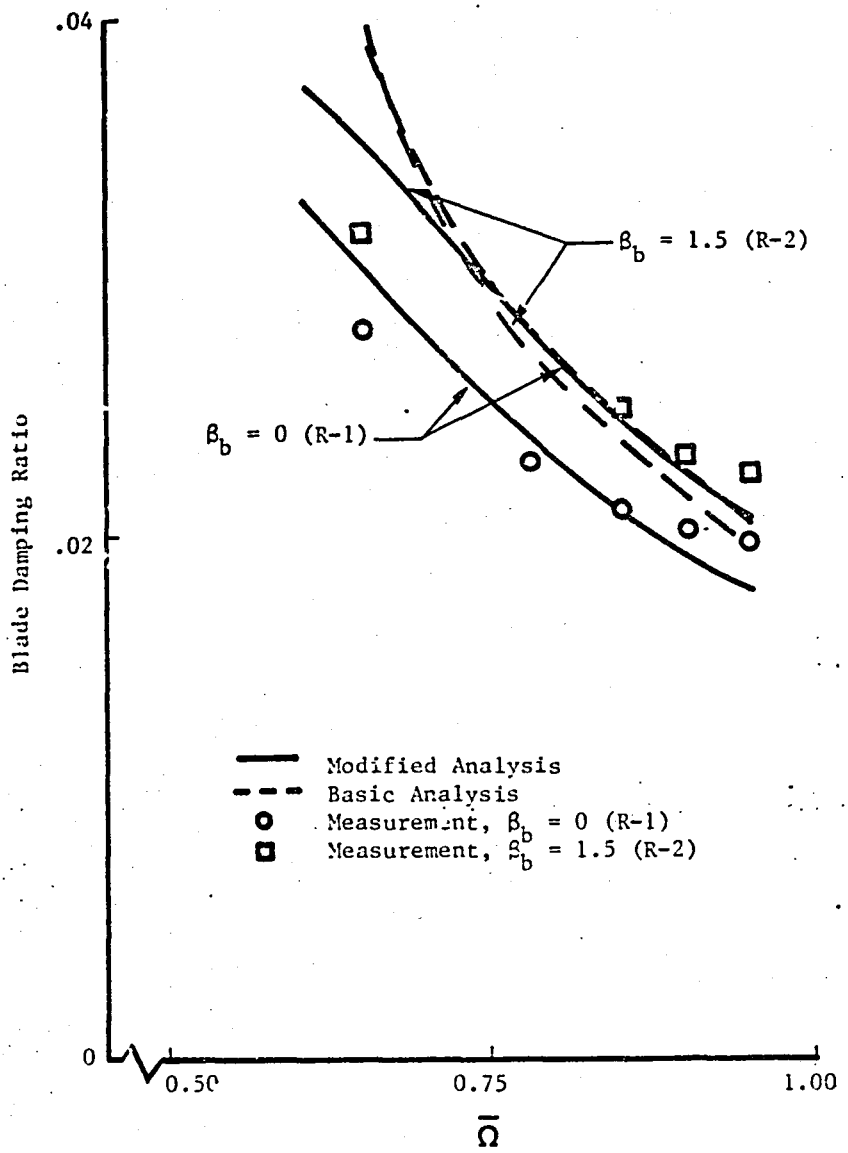

Figure 27. Damping Correlation With Rotor Speed Using the Modified (Transformation) Analysis for Isolated Rotor (T = 1g).

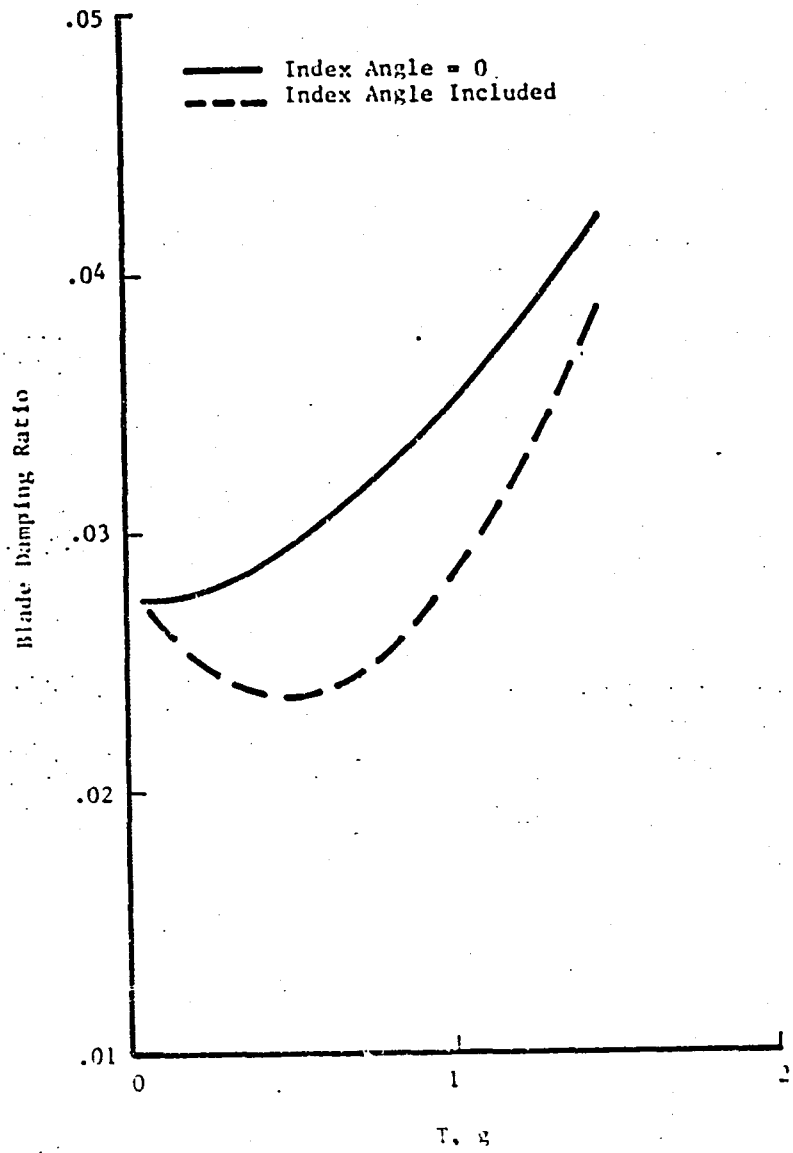

Figure 28. Effect of Cuff Shear Restraint/Inplane Damper Pitch Index as Predicted by Basic Analysis for Isolated Rotor Configuration R-1 ($\bar{\Omega}$ = 0.78).

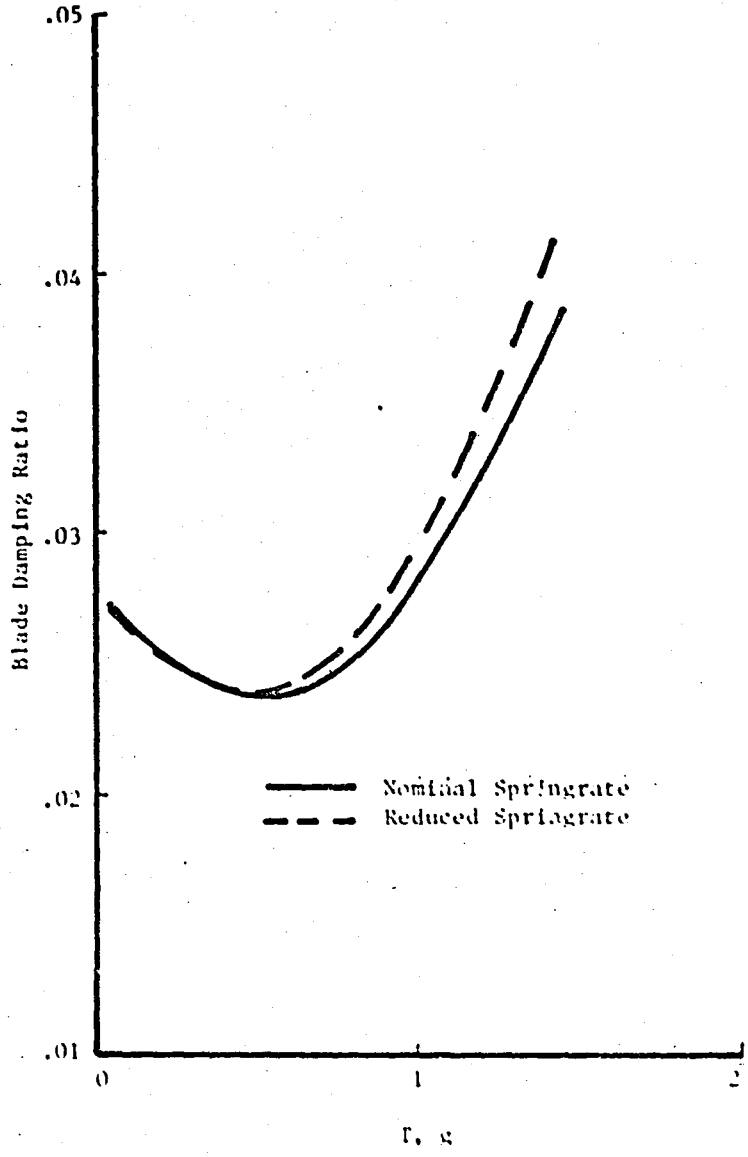

Figure 29. Effect of Control System Springrate on Inplane Damping as Predicted by the Basic Analysis for Isolated Rotor Configuration R-1 ($\bar{\Omega}$ = 0.78).

End of Document